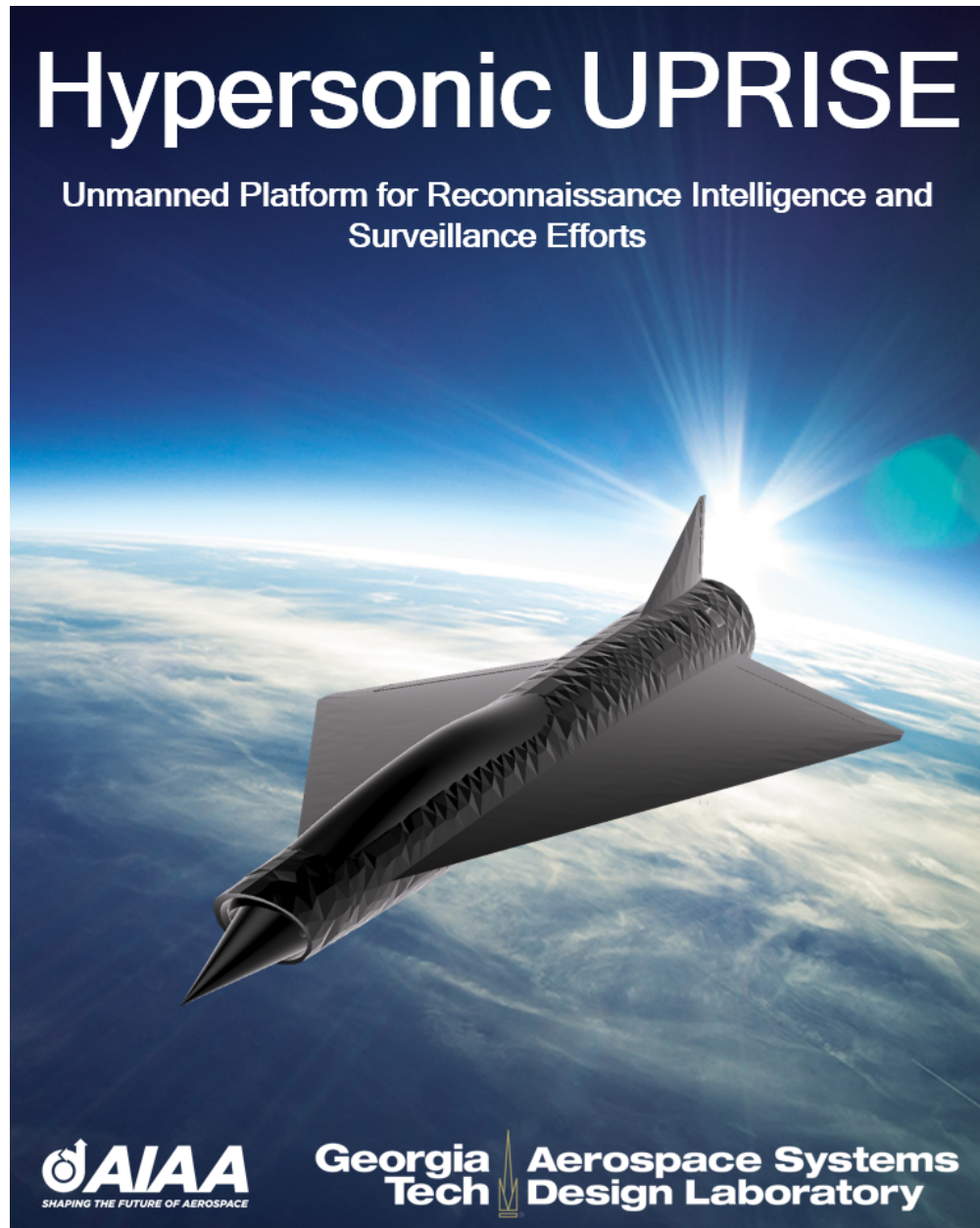


# Design of a Reusable Penetrating Hypersonic Intelligence, Surveillance, and Reconnaissance Platform

William Cammack, Baptiste Cramette, Joey Ji, Antonio Macias, Salil Sodhi, Gowtham Venkatachalam, Tyler Wills,  
Karen Yehoshua

*Aerospace Systems Design Laboratory (ASDL)  
Georgia Institute of Technology, Atlanta, Georgia, 30332, United States*





Dr. Dimitri Mavris  
Faculty Advisor

*Dimitri Mavris*



Dr. Brad Robertson  
Research Advisor

*Brad Robertson*



Dr. Ken Decker  
Research Advisor

*Ken Decker*



William Cammack  
ASDL  
AIAA #: 1345257

*William Cammack*



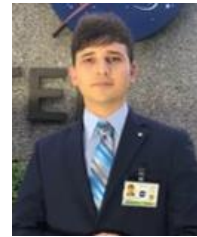
Baptiste Cramette  
ASDL  
AIAA #: 1326111

*Cramette*



Joey Ji  
ASDL  
AIAA #: 936004

*Joey Ji*



Antonio Macias  
ASDL  
AIAA #: 1345823

*Antonio Macias*



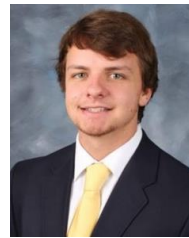
Salil Sodhi  
Undergraduate  
AIAA #: 1345941

*Salil Sodhi*



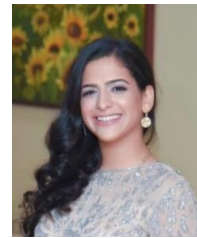
Gowtham Venkatachalam  
ASDL  
AIAA #: 1326081

*Gowtham Venkatachalam*



Tyler Wills  
ASDL  
AIAA #: 1345933

*Tyler Wills*



Karen Yehoshua  
ASDL  
AIAA #: 1356372

*KY*

## I. Nomenclature

$advmat$	=	amount of composites/titanium/high temperature ceramics as percent of structural weight
$a, b, C$	=	Tauber-Sutton radiative heat flux curve fit coefficient
$C_{depreciation}$	=	depreciation cost
$C_l$	=	coefficient of lift
$C_{overhead}$	=	overhead cost
$C_p$	=	coefficient of pressure
$C_f$	=	skin friction coefficient
$C_{fuel}$	=	fuel cost
$C_{maintenance}$	=	maintenance cost
$C_{nEng}$	=	nonrecurring engineering cost
$C_{overhead}$	=	overhead cost
$C_{RDT\&E}$	=	research, development, and testing cost
$C_{sj}$	=	cost of a single scramjet engine
$C_{tj}$	=	cost of a single turbojet engine
$C_{tooling}$	=	tooling cost
$C_{unit}$	=	cost to produce a single vehicle
$C_{vehicle}$	=	total cost of a single vehicle
$C_{vehicle,aq}$	=	vehicle acquisition cost
$coef$	=	cost coefficient as a function of weight
$D$	=	drag
$ff$	=	first flight minus 1950
$h$	=	heat transfer coefficient
$I_{sp}$	=	specific impulse
$g$	=	acceleration due to gravity
$K_{Isj}$	=	ratio of maintenance labor for scramjet engine to current subsonic engines
$K_{Itj}$	=	ratio of maintenance labor for hypersonic turbojets to subsonic aircraft
$K_{msj}$	=	ratio of maintenance material for scramjet engine to current subsonic engines
$K_{mtj}$	=	ratio of maintenance material for hypersonic turbojets to subsonic aircraft
$L$	=	lift
$L_d$	=	depreciable life of the vehicle [year]
$M_c$	=	cruise mach number

$maintenance_{af,l}$	=	maintenance cost of labor for the airframe [Cents/mile-ton]
$maintenance_{af,m}$	=	maintenance cost of materials for the airframe [Cents/mile-ton]
$maintenance_{sj,l}$	=	maintenance cost of labor for the scramjet engine [Cents/mile-ton]
$maintenance_{sj,m}$	=	maintenance cost of materials for the scramjet engine [Cents/mile-ton]
$maintenance_{tj,l}$	=	maintenance cost of labor for the turbojet engine [Cents/mile-ton]
$maintenance_{tj,m}$	=	maintenance cost of materials for the turbojet engine [Cents/mile-ton]
$N_{sj}$	=	number of scramjet engines
$q_{convective}$	=	convective heat flux
$q_{radiative}$	=	radiative heat flux
$R$	=	range
$R_{nose}$	=	vehicle nose radius
$Rate$	=	production rate [aircraft per year]
$Re$	=	Reynolds Number
$r_{eng}$	=	engineering labor rate [\$/hr]
$r_l$	=	maintenance labor rate [\$/hr]
$r_t$	=	tooling labor rate [\$/hr]
$S$	=	wing area
$t_f$	=	time of flight
$T$	=	thrust
$T_{tj}$	=	maximum thrust of a single turbojet
$(T/W)_{gto}$	=	thrust to weight at takeoff
$U_{vehicle}$	=	utilization of the vehicle [hr/year]
$V_b/V_{cr}$	=	ratio of block velocity to cruise velocity
$V, v$	=	velocity
$W_{af}$	=	airframe weight
$W_{av}$	=	avionics system weight
$W_e$	=	empty weight
$W_{gto}$	=	gross takeoff weight
$W_{pl}$	=	payload weight
$W_0$	=	initial weight
$W_f$	=	final weight
$\alpha$	=	angle of attack

$\theta$  = angle between local tangent and freestream

$\phi$  =  $90-\theta$

$\rho$  = density

## Executive Summary

The UPRISE vehicle is an unmanned and reusable hypersonic intelligence, surveillance, and reconnaissance vehicle. UPRISE has a design range of 3,000 nautical miles at a speed of Mach 8 at 100,000 ft. The UPRISE vehicle uses airbreathing propulsion and non-ablative thermal protection materials to meet turnaround time requirements. Without the use of ITAR or export controlled tools, the system design was built from the ground up using first principles. Through the creation and use of a Multidisciplinary Design Analysis (MDA) environment, the highly coupled nature of vehicle design can be captured with feed-forward and feed-back loops until a vehicle converges to meet requirements. The UPRISE vehicle has a unit cost around \$716 million with the total operating costs per sortie at \$395,000. 3-D CAD renderings of the UPRISE vehicle are shown below.



# Contents

<b>I Nomenclature</b>	<b>3</b>
<b>II Introduction</b>	<b>12</b>
II.A Project Introduction . . . . .	12
II.B Background and Existing Systems . . . . .	12
<b>III Requirements</b>	<b>13</b>
III.A Explicit Requirements . . . . .	13
III.B Derived Requirements . . . . .	14
III.C Concept of Operation . . . . .	15
III.D Key Hypersonic Design Challenges . . . . .	16
<b>IV Defining the Concept Space</b>	<b>17</b>
<b>V Modeling and Simulation</b>	<b>20</b>
V.A Geometry Generation . . . . .	21
V.B Weight Analysis . . . . .	24
V.C Propulsion Analysis . . . . .	24
V.D Aerodynamics Analysis . . . . .	26
V.D.1 Subsonic Aerodynamic Analysis . . . . .	27
V.D.2 Geometry Interpretation . . . . .	28
V.D.3 Supersonic Aerodynamic Analysis . . . . .	28
V.D.4 Hypersonic Aerodynamic Analysis . . . . .	30
V.E Mission Analysis . . . . .	34
V.E.1 Takeoff and Climb . . . . .	36
V.E.2 Hypersonic Cruise and High-Speed Turning Flight . . . . .	37
V.E.3 Descent and Landing . . . . .	38
V.F Thermal Protection Analysis . . . . .	39
V.G Cost Analysis . . . . .	40
V.G.1 Maintenance Cost . . . . .	41
V.G.2 Operating Cost . . . . .	43
V.G.3 Vehicle Cost . . . . .	43
V.G.4 Miscellaneous Cost . . . . .	45

<b>VI Design Space Exploration</b>	<b>45</b>
VI.A DoE Inputs/Outputs . . . . .	46
VI.A.1 Surrogates . . . . .	48
VI.A.2 Sensitivities . . . . .	50
<b>VII Vehicle Selection</b>	<b>51</b>
VII.A Overall Design . . . . .	51
VII.B Weight Breakdown . . . . .	53
VII.C Propulsion . . . . .	54
VII.D Aerodynamics . . . . .	56
VII.E Mission Analysis . . . . .	59
VII.E.1 Takeoff . . . . .	59
VII.E.2 Climb . . . . .	59
VII.E.3 Landing Performance . . . . .	61
VII.F Stability and Control . . . . .	63
<b>VIII Conclusion</b>	<b>65</b>



## List of Figures

1	Mission profile . . . . .	16
2	Proven and notional high-speed concepts . . . . .	17
3	Initial morphological matrix . . . . .	18
4	Down selected morphological matrix . . . . .	19
5	Down selected morph matrix with architectures . . . . .	19
6	Down selected configurations . . . . .	20
7	Design structure matrix (DSM) . . . . .	21
8	Fuselage variation . . . . .	22
9	Wing variation . . . . .	23
10	Vertical stabilizer variation . . . . .	23
11	Specific impulse of various jet engines vs mach number . . . . .	25
12	Single horseshoe vortex . . . . .	27
13	Vortex lattice on lifting surfaces . . . . .	27
14	Vehicle triangular mesh . . . . .	28
15	Tangent wedge/tangent cone method . . . . .	29
16	Modified Newtonian aerodynamics . . . . .	30
17	Modified Newtonian angle distinction . . . . .	31
18	Drag polar: mach 5 at 80,000 ft . . . . .	32
19	Pressure contour on a cube . . . . .	32
20	Coefficient of friction in x-direction contour on a cube . . . . .	33
21	Pressure contours with positive angle of attack . . . . .	33
22	Heat transfer coefficient contour: 0 degrees angle of attack . . . . .	34
23	Free body diagram of the aircraft modeled as a point mass . . . . .	35
24	TPS material feasible space . . . . .	40
25	Overall scatter plot matrix . . . . .	48
26	Overall scatter plot matrix: vehicles under 50,000lb . . . . .	49
27	Variable importance . . . . .	49
28	Surrogate fits . . . . .	50
29	Sensitivity analysis . . . . .	50
30	Optimal UPRISE configuration . . . . .	52
31	Internal layout for the UPRISE optimal configuration . . . . .	53
32	Engines location, size, and performance parameters . . . . .	55

33	Performance parameters of the modified J85 turbojet at different flight conditions . . . . .	55
34	Aircraft aerodynamic performance for different flight conditions . . . . .	57
35	Aircraft aerodynamic performance at cruise . . . . .	57
36	Aircraft aerodynamic performance at cruise . . . . .	58
37	Pressure contour: 10 degrees angle of attack . . . . .	58
38	Heat transfer coefficient contour: 0 degrees angle of attack . . . . .	58
39	Heat transfer coefficient contour 0 AoA: RF antenna location . . . . .	59
40	Takeoff and tail strike avoidance . . . . .	60
41	Climb trajectory of the aircraft . . . . .	60
42	Altitude with respect to velocity during climb segment . . . . .	61
43	Landing gear location and dimensions . . . . .	61
44	Generic landing profile . . . . .	62
45	Control surfaces size and location . . . . .	64

## List of Tables

1	ISR alternatives . . . . .	12
2	Explicit requirements . . . . .	14
3	Derived requirements . . . . .	15
4	Flight conditions DoE ranges . . . . .	46
5	Vehicle parameters DoE ranges . . . . .	47
6	Selected vehicle parameters . . . . .	51
7	Selected vehicle parameters . . . . .	53
8	Vehicle weight breakdown by component and category . . . . .	54
9	Static stability analysis . . . . .	64
10	UPRISE compliance to RFP requirements . . . . .	65

## II. Introduction

### A. Project Introduction

This report outlines the Georgia Institute of Technology Missile Design Team’s final vehicle design for the 2021-2022 American Institute of Aeronautics and Astronautics (AIAA) Graduate Team Missile Systems Design Competition. AIAA hosts this competition annually and provides a Request for Proposal (RFP) for a missile system with the potential for real-life applications. However, for the 2021-2022 competition, the RFP does not call for a missile system but rather a reusable, penetrating, hypersonic intelligence, surveillance, and reconnaissance (ISR) platform. This report provides a detailed description and discussion of the design process, design environment, and final design of the Hypersonic UPRISE vehicle.

### B. Background and Existing Systems

While intelligence, surveillance, and reconnaissance vehicles are not a new concept to the military, ISR platforms have certainly evolved over time. ISR vehicles began as manned subsonic aircraft, such as the U-2. However, as needs for faster data acquisition and greater survivability increased, supersonic ISR vehicles, like the SR-71, came to fruition. When needs changed, the SR-71 program was retired but still remains the fastest ISR vehicle to this day. Since then, ISR vehicles have taken the form of unmanned subsonic aircraft, such as the RQ-4 Global Hawk, and satellites, such as those in the DARPA Blackjack program. Table 1 weighs some of the benefits and challenges of each ISR platform.

**Table 1** ISR alternatives

	<b>Benefits</b>	<b>Challenges</b>
<b>Satellite ISR</b>	Large survey area Low-risk	Cannot be quickly deployed Only effective when in range
<b>Subsonic ISR</b>	Long flight time Multiple sensor types	Struggle to meet time-critical needs Easily detectable Prone to interception
<b>Supersonic ISR</b>	Can be deployed rapidly Quickly gather sensitive information	Costly to operate and manufacture Struggles to meet time-critical needs

Note: Supersonic ISR has been retired for 20 years

Evaluating the ISR alternatives in Table 1, it is evident that no alternatives meet the time-critical needs; thus, there is a capability gap for a reusable, unmanned hypersonic ISR platform. An additional need for hypersonic ISR is survivability. As noted in the table, current subsonic ISR platforms are prone to interception due to the advancement of surface to air missiles such as the S-400 Triumf. With a hypersonic ISR capability, there is a lower likelihood of being intercepted.

Currently, unmanned and reusable hypersonic ISR vehicles have yet to be produced and fielded by the United States and its allies. The closest relative to this effort is the SR-71 Blackbird which had cruise speeds exceeding Mach 3.

Experimental hypersonic demonstrators, like the X-15, X-51, and X-43, have been produced but have not been applied to ISR missions. Additionally, of the existing hypersonic vehicles that have been produced, none were fully reusable or capable of meeting a 24-hour turn around time.

### **III. Requirements**

This section will outline the explicit requirements, the derived requirements, and the proposed concept of operations for the UPRISE hypersonic vehicle.

#### **A. Explicit Requirements**

Provided by AIAA, the request for proposal (RFP) outlines explicit requirements concerning flight performance, operations, production specifications, and service dates [1].

Looking first at performance requirements, the hypersonic vehicle shall have a threshold cruise speed of Mach 5 with an objective cruise speed of Mach 8. It shall have a cruise altitude threshold of 80,000 ft with an objective cruise altitude of 100,000 ft. The vehicle shall have a threshold range of 2,500 nmi with an objective of 3,000 nmi. Lastly, the vehicle shall be capable of landing on conventional paved runways with a field length not to exceed 8,000 ft. In terms of operation requirements, the vehicle shall be reusable with a turn around time of less than 24 hours between sorties. The vehicle shall be capable of round trip or one way missions. The vehicle shall also be unmanned using remote pilot controls with an optional autonomous cruise.

In terms of mission and program requirements, the vehicle shall be capable of carrying an ISR payload with dimensions of 3 ft by 3 ft by 12 ft and an approximate weight of 1,000 lb. Two downward facing windows are required with each being 12 inches in diameter, EO/IR transparent, and contiguous to the payload space allocation. At least 2,000 Watts of power shall be available to power the ISR equipment. The vehicle shall also accommodate a 1 ft by 2 ft RF antenna located on either side of the fuselage with minimal heat flux exposure. As far as programmatic requirements, per the RFP, development shall start in October 2022 with initial operational capability (IOC) no later than December 2030. Five aircraft and two ground stations shall be produced for research, development, test, and evaluation (RDT&E) after which 10 aircraft and 2 ground stations shall be produced every year for 10 years. Table 2 below tabulates the explicit requirements listed above.

**Table 2 Explicit requirements**

	<b>Requirements</b>
<b>Cruise Speed</b>	Threshold: Mach 5 Objective: Mach 8
<b>Range</b>	Threshold: 2,500 nmi Objective: 3,000 nmi
<b>Cruise Altitude</b>	Threshold: 80,000 ft Objective: 100,000 ft
<b>Runway Field Length</b>	Max Length = 8,000 ft Conventional Paved Runway
<b>Reusable</b>	Turn around time between sorties < 24 hrs
<b>Unmanned</b>	Remotely Piloted Optional Autonomous Cruise
<b>Mission Profile</b>	Capable of one way and round trip
<b>ISR Payload</b>	Dimensions: 3' x 3' x 12' Weight: 1000 lb 2 Downward facing windows: 12" diameter Windows: EO/IR transparent, and contiguous to payload space Power Required: 2000 Watts
<b>RF Antenna</b>	Window size: 1' x 2' Location: Either side of fuselage
<b>Production Run</b>	RDTE: 5 aircraft and 2 ground stations 10 year production run: 10 aircraft/year and 2 ground station/year IOC no later than 12/2030

**B. Derived Requirements**

To meet the explicit requirements outlined in the RFP, additional requirements for the vehicle are derived. A majority of the derived requirements stem from the operational requirements. Perhaps the most critical derived requirement concerns the explicit requirements of reusability and 24 hour turn around time between sorties. The explicit requirement brings into question the definition of reusability. According to NASA [2], reusability can be divided into two facets. The first facet is partial reusability. Partial reusability states that parts of the system are reusable, however some components must be repaired or replaced between missions. An example of partial reusability would be the NASA space shuttle. On the other hand, full reusability states that the entire system can be reused without any replacement or refurbishment of parts between each sortie. The closest applicable example of full reusability would be a commercial airliner. Given the established definition of reusability, it is permissible for the vehicle to be partially reusable as long as the 24 hour turn around time between sorties can be met. This derived requirement comes with many subsequent considerations. In propulsion, rocket boosters cannot be exchanged in the time allotted between sorties, thus limiting propulsion to be air-breathing and fully reusable. As for thermal protection, ablative materials cannot be used because the heat shield

cannot be replaced in under 24 hours. The reusability derived requirement extends beyond the vehicle itself. Any support equipment necessary for vehicle operations shall be available and/or capable of reuse within the 24-hour vehicle turn around requirement.

Along with the explicit reusability requirement, additional operational requirements are derived. In terms of service life, no requirements were stated in the RFP. Looking at previous programs, such as SR-71 [3], the requirement is derived that the vehicle shall be able to perform 2,000 flight hours before decommissioning. In terms of logistics, the requirement is derived that the vehicle shall use hydro-carbon fuel due to its availability and established supply chains.

Technical requirements must also be derived to fulfill the explicit requirements set in the RFP. One of the primary challenges of this vehicle and its mission is thermal protection. A key challenge with hypersonic flight is preventing communication blackout and overheating. The requirement is derived that the vehicle shall have sufficient thermal protection systems to ensure communication equipment is not damaged and signal can be maintained. Additionally, the vehicle will be subjected to hypersonic thermal soak for a significant portion of the mission. The requirement is derived that the vehicle shall have appropriate thermal protection systems to accommodate at least 40 minutes of hypersonic flight. The 40 minute value is calculated as the time to fly a distance of 2000 nautical miles at a speed of Mach 5.

Another derived requirement concerns the weight of the subsystems in the vehicle. In terms of electrical power, the vehicle shall be able to provide 2000W of electrical power by means of engine bleed or batteries. Additionally, the navigation system must be operational in the event that GPS signaling and communications are denied by the adversary. Both of these derived requirements, only account for weight impacts to the vehicle. No electrical power or GPS signal models are used. Table 3 below shows the most notable derived requirements for the vehicle design.

**Table 3 Derived requirements**

<b>Technical Requirements</b>	TPS must ensure communication equipment is not damaged and signal can be maintained TPS must accommodate 40 minutes of hypersonic flight The navigation system must be operational in a denied environment
<b>Operational Requirements</b>	Partially reusable as long as the 24 hour turn around time between sorties can be met Any support equipment must meet 24-hour vehicle turn around requirement Perform 2,000 flight hours before decommissioning Use hydro-carbon fuel due to its availability and established supply chains

### C. Concept of Operation

The UPRISE vehicle will be used to perform intelligence, reconnaissance, and surveillance missions at greater speeds than its subsonic counterparts. As discussed in the previous section, the vehicle will be unmanned and reusable. The vehicle will be capable of one way or round trip missions and operable at existing air bases.

The military of the United States and its allies could be a potential user of the UPRISE vehicle. To operate the vehicle, a team of operators is required. Most notably, a pilot is needed to remotely fly the aircraft, an analyst is needed

to collect and interpret data from the sensors, and a ground crew is needed to perform maintenance and operations.

For the missions specified in the RFP, the UPRISE vehicle concept of operations is shown below.

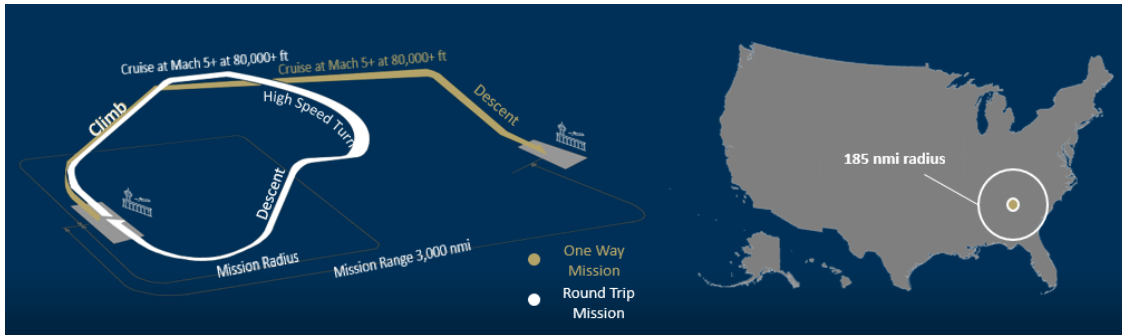


**Fig. 1 Mission profile**

As shown in the figure, this vehicle must be able to perform both a one-way and round-trip mission. One key observation to make with the round-trip mission is the high-speed turn. To put the turn into perspective, if the vehicle is travelling at the objective cruise speed, Mach 8, and could sustain a 2g turn, the minimum turn radius would be 185 nmi. Thus, a large portion of the round-trip mission must be dedicated to the high-speed turn.





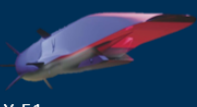

#### **D. Key Hypersonic Design Challenges**

Having the requirements of the competition in mind, the key hypersonic design challenges are identified. The largest of these challenges are primarily found in the disciplines of propulsion, aerodynamics, and thermal protection systems. The most notable challenge with propulsion is selecting an airbreathing engine(s) that is capable of both subsonic takeoff and landing, hypersonic cruise, and everything in between. Due to the wide range in Mach number throughout the mission profile, multiple engines must be used. Certain engine types are only compatible at specific flow regimes, such that the propulsion system must be carefully down selected to include the minimum number of engines that are capable of supporting the defined mission profile. Typically, this hurdle can be avoided by using rocket boosters. However, boosters do not meet the reusability requirement, so they may not be utilized in this design. The next set of challenges lie in aerodynamics. Under aerodynamics, the subsonic, transonic, supersonic, and hypersonic flow regimes must all be accounted for. With each flow regime, aerodynamics must be compatible with both the propulsion system and geometry. In this particular competition, there is the added challenge that no ITAR tools may be used to conduct any of the analysis. In addition to the challenges presented in the propulsion and the aerodynamics disciplines, it is also extremely challenging to down select a viable thermal protection system. A thermal protection system is essential in hypersonic vehicle design in order to prevent excessive heating which can cause communication blackout and structural degradation. However, the requirement of reusability prevents the usage of ablative materials for the thermal protection system, since they may not be replaced within the 24 hours between sorties as required by the RFP.



## IV. Defining the Concept Space

After defining the requirements, the concept space can be defined. The concept space looks at features from existing hypersonic and supersonic vehicles to serve as baselines. These aircraft include SR-71, XB-70, X-15, X-51, X-43, and D-21. Additionally, some configurations still in development, such as the Hermeus Quarterhorse, Boeing Hypersonic Airliner, and Hypersonix/Kratos DART, are included in the analysis. Refer to Figure 2 to review some of the considered concepts and their physical attributes.

Proven		Notional Concepts	
 XB-70	<b>Max Speed: Mach 3</b> Tube and Wing Delta Wing Podded Engine Twin Tail	 Hermeus Quarterhorse	<b>Max Speed: Mach 5</b> Tube and Wing Delta Wing Integral Engine Single Tail
 Lockheed D-21	<b>Max Speed: Mach 3</b> Tube and Wing Delta Wing Rocket Boosted / Ramjet Single Tail	 Boeing Hypersonic Airliner	<b>Max Speed: Mach 5</b> Tube and Wing Delta Wing Podded Engine Twin Tail
 X-51	<b>Max Speed: Mach 5</b> Waverider Podded Engine Rocket Boosted V-Tails	 Kratos/Hypersonix DART AE	<b>Max Speed: Mach 5-12</b> Tube and Wing Delta Wing Podded Engine V-tail

**Fig. 2 Proven and notional high-speed concepts**

As shown in the figure above, it can be seen that the mission requirements cannot be met by derivative concepts of proven vehicles. Consequently, a method is needed to map potential vehicle configurations to the requirements. This can be done through a morphological matrix. The purpose of the morphological matrix is to consider many alternatives, both mature and developing, in order to keep the concept space as encompassing as possible. In performing this exercise, the initial morphological matrix can be shown in Figure 3.

While the approach is rather simple, the morphological matrix contains millions of potential combinations. Even if computation time is as quick as one second per configuration, the time to compute all alternatives would take years. Thus, it is not feasible to conduct a study on every combination. The morphological matrix must be down selected to reduce the dimensionality of the problem. Listed below are the down selections with a brief justification. A down selected morphological matrix is shown in Figure 4.

- Blended wing body and lifting body are eliminated due to historical precedent and low performance in high-speed flight.
- In wing planform, the waverider configurations are eliminated due to its high approach speeds and poor low speed aerodynamic performance.

<b>Vehicle Configuration</b>	Configuration	Tube and Wing	Blended Wing Body	Lifting Body		
	Fuselage	Sears Hack	Cone			
	Wing Planform	Delta	Tapered	Double-Delta	Waverider	
	Wing Sweep	Aft Sweep	Variable Sweep			
	Empennage	Conventional	V-tail	Twin Tail	None	
<b>Controls</b>	Pitch Control	Elevators	Ruddervators	Elevons		
	Yaw Control	Rudder	Ruddervators			
	Roll Control	Ailerons	Elevons			
<b>Propulsion</b>	Engine Types	Turbojet + Ramjet	Turbojet + Ramjet + Scramjet	Booster + Ramjet	Booster + scramjet	Booster + Ramjet + Scramjet
	Engine Location	Inside the Fuselage	Under Fuselage	Under Wing		
<b>Subsystems</b>	Braking System at Landing	Traditional Brakes	Brakes with Spoilers	Brakes with Spoilers and Drogue Parachute		
	Power Generation	Battery	Engine Bleed			
	Pilot Operability	Synthetic Vision + Instrument	Instrument Only	Autonomous		
<b>Materials</b>	TPS	High Temperature Materials	+ Active Cooling			
	Wing Materials	Titanium	Nickel Alloys	Ceramic Composites	High Temp Ceramics	Hybrid
	Fuselage	Titanium	Nickel Alloys	Ceramic Composites	High Temp Ceramics	Hybrid

**Fig. 3 Initial morphological matrix**

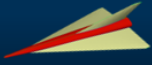



- Variable wing sweep is eliminated due to its over complexity, specifically with respect to structural considerations.
- V-tail and tailless configurations are eliminated due to historical precedent and concerns of stability and control.
- Since V-tails were eliminated, so too are ruddervators. Additionally, traditional ailerons and elevators are eliminated as the wing planform is simplified to a delta or tapered wing.
- In propulsion, rocket boosters are eliminated due to the reusability and turn around requirements.
- For engine location, under the wing is eliminated do to the forebody compression from the fuselage needed to operate ramjet or scramjet engines.
- In the thermal protection system, active cooling is eliminated due to increased complexity and its difficulties to manufacture.

In the figure, eliminated fields are marked in grey. As shown, not every category could be down selected thus a trade study must be performed with these variables to evaluate their feasibility. Assessing the possible combinations after down selection, two configurations emerge as shown in Figure 5.

These two configurations are named "UPRISE 1" and "UPRISE 2." UPRISE 1 takes its inspiration from the Hermeus Quarterhorse and UPRISE 2 is inspired by the Boeing Hypersonic Airliner, both of these notional configurations match the closest to the requirements. Looking at the configurations in more detail, UPRISE 1 is a tube and wing design with a single tail, one buried engine, one podded engine, and a conical inlet. The benefits to this configuration are low speed performance and relatively few thin leading surfaces that could limit overheating. However, with a buried engine, special consideration must be made to how the subsystems are packaged with the integral flow path. Looking at

<b>Vehicle Configuration</b>	Configuration	Tube and Wing	Blended Wing Body	Lifting Body		
	Fuselage	Sears Hack	Cone			
	Wing Planform	Delta	Tapered	Double-Delta	Waverider	
	Wing Sweep	Aft Sweep	Variable Sweep			
	Empennage	Conventional	V-tail	Twin Tail	None	
<b>Controls</b>	Pitch Control	Elevators	Ruddervators	Elevons		
	Yaw Control	Rudder	Ruddervators			
	Roll Control	Ailerons	Elevons			
<b>Propulsion</b>	Engine Types	Turbojet + Ramjet	Turbojet + Ramjet + Scramjet	Booster + Ramjet	Booster + scramjet	Booster + Ramjet + Scramjet
	Engine Location	Inside the Fuselage	Under Fuselage	Under Wing		
<b>Subsystems</b>	Braking System at Landing	Traditional Brakes	Brakes with Spoilers	Brakes with Spoilers and Drogue Parachute		
	Power Generation	Battery	Engine Bleed			
	Pilot Operability	Synthetic Vision + Instrument	Instrument Only	Autonomous		
<b>Materials</b>	TPS	High Temperature Materials	+ Active Cooling			
	Wing Materials	Titanium	Nickel Alloys	Ceramic Composites	High Temp Ceramics	Hybrid
	Fuselage	Titanium	Nickel Alloys	Ceramic Composites	High Temp Ceramics	Hybrid

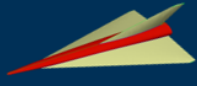

**Fig. 4 Down selected morphological matrix**

<b>Vehicle Configuration</b>	Configuration	Tube and Wing	Blended Wing Body	Lifting Body			
	Fuselage	Sears Hack	Cone				
	Wing Planform	Delta	Tapered	Double-Delta	Waverider		
	Wing Sweep	Aft Sweep	Variable Sweep				
	Empennage	Conventional	V-tail	Twin Tail	None		
<b>Controls</b>	Pitch Control	Elevators	Ruddervators	Elevons			
	Yaw Control	Rudder	Ruddervators				
	Roll Control	Ailerons	Elevons				
<b>Propulsion</b>	Engine Types	Turbojet + Ramjet	Turbojet + Ramjet + Scramjet	Booster + Ramjet	Booster + scramjet	Booster + Ramjet + Scramjet	
	Engine Location	Inside the Fuselage	Under Fuselage	Under Wing			
<b>Subsystems</b>	Braking System at Landing	Traditional Brakes	Brakes with Spoilers	Brakes with Spoilers and Drogue Parachute			
	Power Generation	Battery	Engine Bleed				
	Pilot Operability	Synthetic Vision + Instrument	Instrument Only	Autonomous			
<b>Materials</b>	TPS	High Temperature Materials	+ Active Cooling				
	Wing Materials	Titanium	Nickel Alloys	Ceramic Composites	High Temp Ceramics	Hybrid	
	Fuselage	Titanium	Nickel Alloys	Ceramic Composites	High Temp Ceramics	Hybrid	
<b>UPRISE 1</b>		<b>UPRISE 2</b>					
<b>Generic Configuration</b>		<b>Inspiration</b>		<b>Generic Configuration</b>		<b>Inspiration</b>	
							
		<b>Hermeus Quarterhorse</b>				<b>Boeing Hypersonic Airliner</b>	

**Fig. 5 Down selected morph matrix with architectures**

UPRISE 2, this is also a tube and wing configuration with a twin tail, two podded engines, and a rectangular inlet. This configuration benefits from simple forebody compression, simplified thermal management without integral engines, and more options to place ISR payload. However, this configuration could prove to have many hotspots due to localized heating on the many leading edge surfaces. The descriptions of the two configurations can best be shown in Figure 6.

While down selecting to two configurations greatly decreases the dimensionality of the categorical concept space,

Configuration		
	UPRISE 1	UPRISE 2
Lift Generation	Tube and Wing	Tube and Wing
Lateral Stability	Single Tail	Twin Tail
# Engines	2	2
Engine Location	In Fuselage/Podded	Both Podded (like the XB-70)
Inlet Architecture	Conical	Rectangular
Design Considerations	<ul style="list-style-type: none"> <li>- Potential for better low speed performance</li> <li>- Few thin leading surfaces</li> <li>- Difficult to fit subsystems with an integral flow path</li> </ul>	<ul style="list-style-type: none"> <li>- Simple forebody compression</li> <li>- Under fuselage engines simplify thermal management</li> <li>- More options for downward facing ISR placement</li> </ul>

**Fig. 6 Down selected configurations**

the continuous concept space must be assessed. With each selected architecture, there is an infinite continuous concept space depending on the variable ranges chosen and the level of granularity in the analysis. The challenge is that there is no empirical data available to narrow the infinite continuous design space, so a method is needed to effectively sample the concept space and perform tradeoffs across architectures. To sample the design space, a design of experiments (DoE) can be used to minimize the number of cases required to explore the design space of a specific vehicle configuration. However, once the concept space is sampled, there is still a need to perform analysis on the sample. This analysis can be done through a modeling and simulation design environment.

## V. Modeling and Simulation

After defining the concept space, there is a need to perform trade studies on the different configurations. To perform these trades and size the vehicle, a design environment must be created. To best display how the environment works, a Design Structure Matrix (DSM) can be made as shown in Figure 7. Following the diagonal boxes in blue and yellow, are the disciplines. The nodes represent outputs that feed forward or backward into the next discipline.

As shown in the diagram, hypersonic vehicle design is an incredibly coupled problem. Almost every discipline is connected to one another. It is important to note that as the environment loops through the cases of the DoE, certain requirement considerations are built in. For example when the DoE gives the environment a range and Mach number, the environment will loop through the sizing and synthesis until a vehicle is found to fit the inputs. Thus, if a design iteration converges it already meets many requirements.

The subsequent sections step through the DSM and details the technical approach and first order principles behind each discipline in the hypersonic vehicle environment. While the disciplines are laid out in a linear fashion the analysis is not performed in this exact linear order due to the highly coupled nature of the problem.

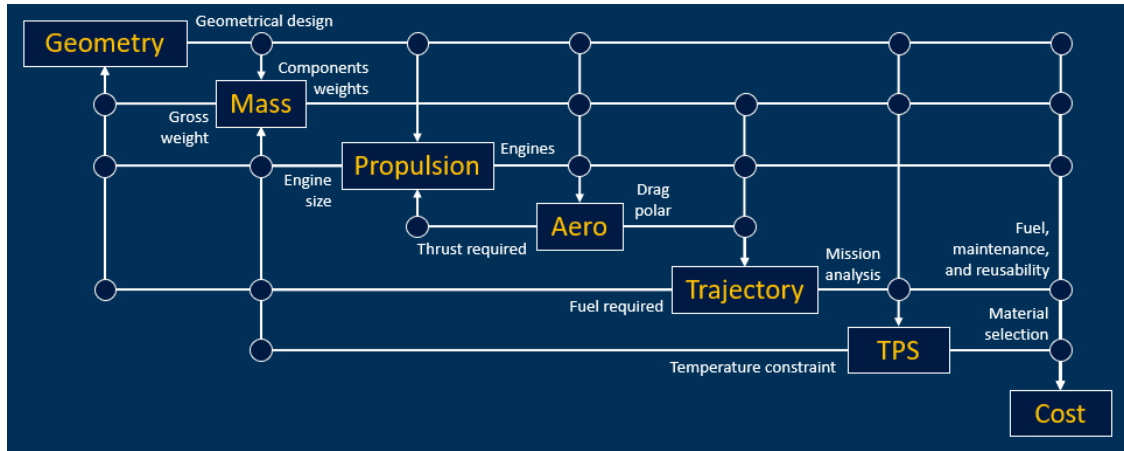


**Fig. 7 Design structure matrix (DSM)**

### A. Geometry Generation

Although the architectures have been down selected to UPRISE 1 and UPRISE 2, there are still multiple needs from the geometry analysis. First, the geometry module needs to be able to convert DoE inputs (scaling parameters, wing sweeps, tail volume coefficients, etc.) and feedback from the MDA environment (fuel volume, engine dimensions, etc.) into watertight geometries to be passed forward to the subsequent disciplines. The geometry module is also needed to be integrated seamlessly with the other disciplinary analyses.

Having identified the needs of the geometry analysis, the various tools to complete the analysis can be assessed. Listed below are the tools to consider.

- Open Vehicle Sketchpad (OpenVSP)
- Engineering Sketchpad (ESP)
- Solidworks

Assessing the options, OpenVSP provides an intuitive user interface oriented towards air vehicle geometry modeling. However, OpenVSP is typically inconsistent at producing watertight geometries. Solidworks provides the largest selection of modeling operations but is more capable than what is required for "in the loop" modeling and is difficult to integrate into the MDA environment. ESP utilizes text files to define geometries, making it cumbersome to use, however it also provides flexible input and output calculations. It also consistently generates watertight geometries. Thus, ESP is the preferred geometry modeling option.

In the UPRISE 1 configuration, the fuselage contains the fuel and ISR payload. The fuselage is resized to meet the volume requirements. The volume for the structure and other components is accounted for by a volumetric efficiency defined as:  $(\text{volume of fuel} + \text{volume of payload}) / \text{fuselage volume}$ . The fuselage is resized to ensure sufficient fuel volume. Additionally, the geometry of the fuselage is controlled by following parameters:

- Cross section height to width ratio

- Nose radius
- Fineness ratio
- Fuel fraction
- Gross weight

Varying the preceding parameters allows the team to explore the fuselage design space of the UPRISE 1 configuration as seen in Figure 8

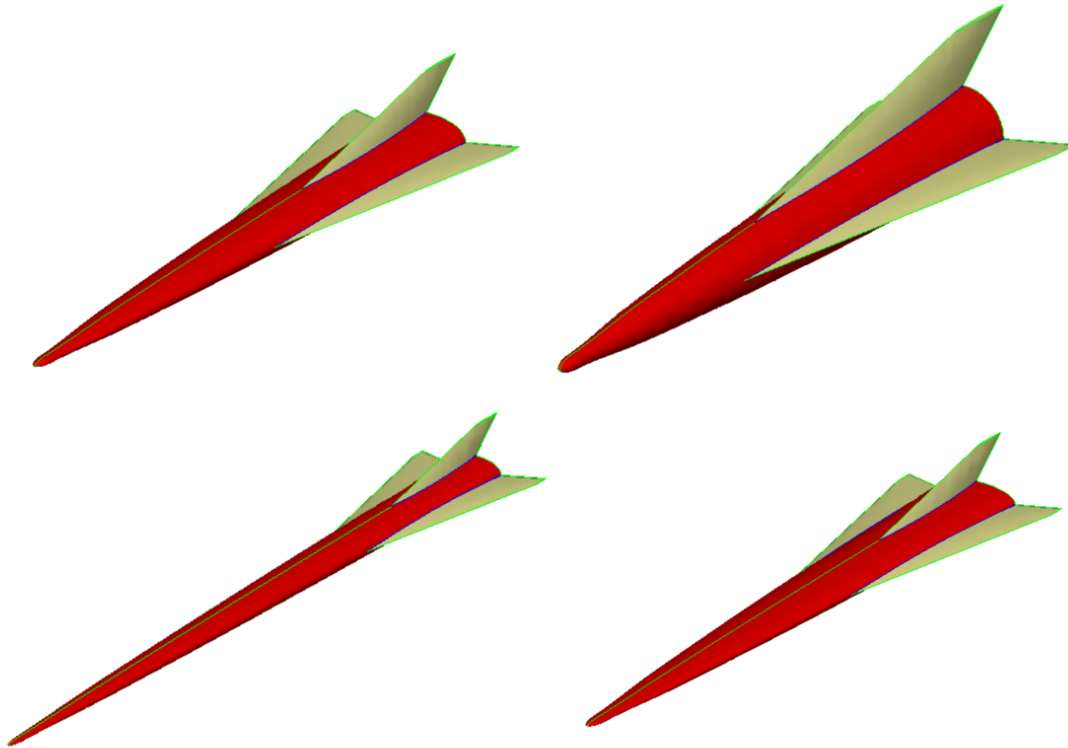


**Fig. 8 Fuselage variation**

The wing of UPRISE 1 is a simple delta wing with a biconvex airfoil throughout. The wing is increased and decreased in size to meet the wing loading target. It is resized by calculating the exposed wing platform area. The geometry of the wing is controlled by following parameters:

- Aspect ratio
- Taper ratio
- Quarter chord sweep
- Dihedral
- Thickness to chord (Root and tip)
- Camber (Root and tip)

- Incidence (Root and tip)

Varying the preceding parameters allows the team to explore the wing design space of the UPRISE 1 configuration as seen in Figure 9

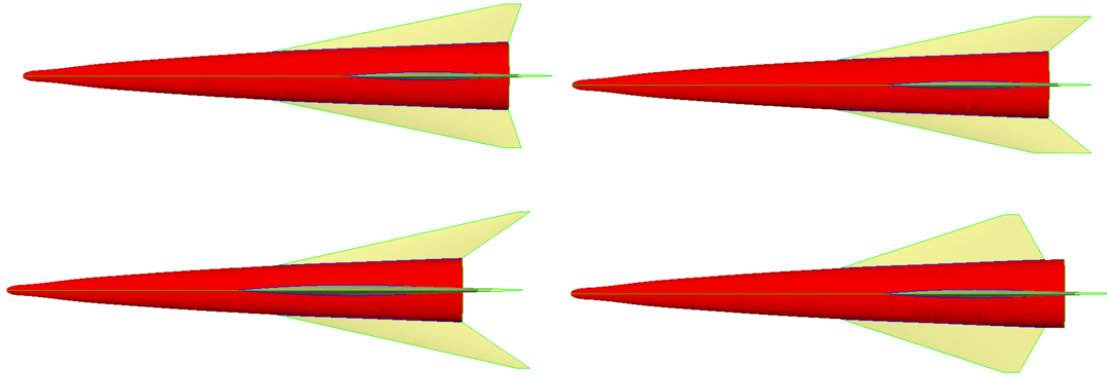


**Fig. 9 Wing variation**

UPRISE 1 has a single taper vertical stabilizer with a biconvex airfoil. It is resized by calculating the exposed vertical stabilizer area and estimating the aerodynamic center of the wing and vertical stabilizer. Additionally, the vertical stabilizer increases or decreases in size to meet the tail volume coefficient target. The geometry of the vertical stabilizer is controlled by following parameters:

- Aspect ratio
- Taper ratio
- Quarter chord sweep
- Dihedral
- Thickness to chord (Root and tip)
- Camber (Root and tip)
- Incidence (Root and tip)

Varying the preceding parameters allows the team to explore the vertical fin design space of the UPRISE 1 configuration as seen in Figure 10

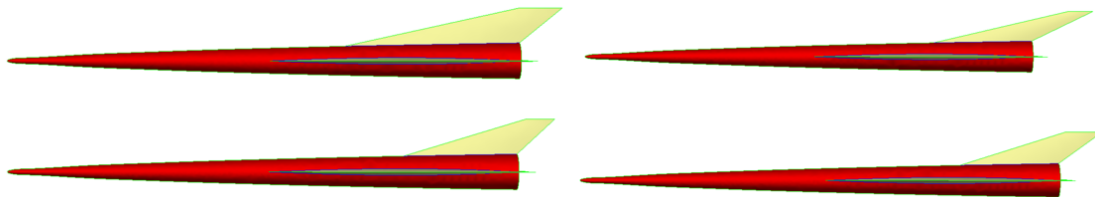


**Fig. 10 Vertical stabilizer variation**

Once the geometry is generated, ESP outputs values such as wing area, surface area, overall dimensions, and volume for weight and cost calculations. It also outputs a surface mesh of the geometry as a .tri file for aerodynamic analysis.

## **B. Weight Analysis**

One of the first steps of conceptual design is to estimate the mass of the vehicle and that of its components. Normally, this is easily enabled through history where a new aircraft can be designed by starting from an existing baseline and infusing technologies. However, given the lack of existing hypersonic vehicles, there are not many available options, and those that are available are inherently inaccurate. Nonetheless, among the best methods to estimate the mass of hypersonic vehicles is the Hypersonic Aerospace Sizing Analysis (HASA) for the preliminary design of aerospace vehicles which was developed by NASA. HASA provides a set of historical regressions that provide mass estimations up to the component level allowing the mass modeling of individual components that later can be used to estimate their position on the aircraft in order to perform a stability analysis. HASA also provides a model for the size of the vehicle but the use of ESP as described in the previous section allows obtaining a higher fidelity structural model. Therefore, the team's use of HASA only involves using the weights model. HASA regressions were built using existing hypersonic vehicles and concepts. However, these vehicles are not very aligned with our design given that they are mostly orbital class vehicles, gliders, and transport concepts that weight hundreds of thousands of pounds. Since the UPRISE concept is much more simplified, it is expected that its gross weight be around 50000 lb (such that the payload weight is ~ 2% of the gross weight similar to the SR-71). Therefore, the weights for the UPRISE components will most likely be determined by extrapolating from HASA, which inherently introduces a source of error. Even though uncertainty is a key consideration, the other models are not as comprehensive as HASA (e.g., they do not model the weight of individual disciplines and components) and even new approaches rely on HASA such as the Physics Informed Neural Networks method, as well as many other Artificial Intelligence and Computer Science methods [4].

## **C. Propulsion Analysis**

In the propulsion analysis, the chosen propulsion system must be airbreathing (as stated in the derived requirements) and capable of resizing "in the loop" based on geometry, weight, aerodynamics, and flight conditions. Detailed below are the considerations to perform the propulsion analysis.

In the past, the vehicles considered to be hypersonic used rocket boosters to reach hypersonic speeds or were carried up to those speeds using a mothership, where they then relied on a scramjet to continue their mission (i.e., the X-51) [5]. Since the reusability requirement limits the design to air breathing propulsion systems, the propulsion discipline brings one of the most complex challenges for the UPRISE concept because it creates the necessity of bringing on board multiple engines. This is because, by design, engines types are limited by their operating conditions (e.g., Mach Number and altitude) as seen in Figure 11 [6]. These limits are imposed by the engine cycle of the different engines



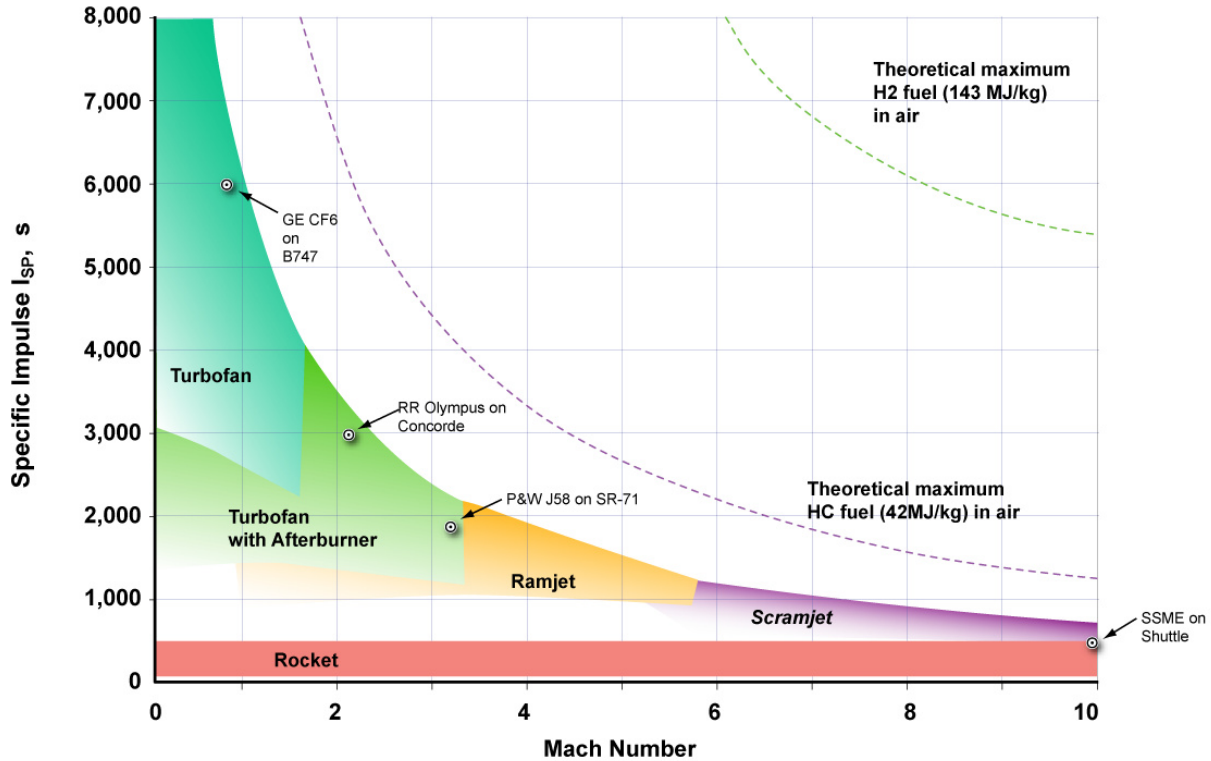


**Fig. 11 Specific impulse of various jet engines vs mach number**

types. This figure also shows that there are many possible combinations to reach subsonic and supersonic speeds but very few to reach hypersonic speeds. Below, we explore the advantages and disadvantages of the possible combinations and justify the selection of the UPRISE propulsion system.

There are three main combinations of engines that will work relatively well to accelerate the aircraft to the design conditions: Low-bypass turbofan + Scramjet, Turboramjet + Scramjet and Turbojet + Dual-Mode Scramjet.

The first combination is not an optimum configuration because even though the low-bypass turbofan ( $\beta=1-2$ ) has a higher propulsive efficiency, it also has a higher drag penalty associated with a large frontal area. This is a major drawback at very high Mach numbers given that the objective is to optimize overall system performance, not just the propulsion system. If the engine is "buried" and the airframe can accommodate the volume of a low-bypass turbofan without increasing drag significantly, it could certainly be a good option. In this case, a mixed stream turbofan (which is inherently harder to analyze) would be considered because the pressure ratio across the fan depends on the operating conditions of the core (assuming that the bypass flow is required to mix with the core flow for afterburner operation, otherwise the engine cannot take us to high supersonic speeds).

The second option is not practical because in order to have a true turboramjet, it is impossible to move the compressor and turbine out of the flow path to transition from turbojet to ramjet operation. Today, this is actually called a turboramjet,

similar to the J58 engine in the SR-71 Blackbird, where air would be bled from the fourth stage of the compressor into the afterburning chamber to simulate ramjet operation. This technology is however 50+ years old and besides the J58, there are no other engines that use a similar cycle.

The third option is the one that most likely will provide the better performance. Here, the turbojet would accelerate the aircraft to Mach 3+, then the inlet to the turbojet flow path is covered and the inlet to the (sc)ramjet flow path is opened and the (sc)ramjet takes over. The ramjet inlet/scramjet isolator section would be designed so that the oblique shock train with final strong oblique or normal shock at lower flight Mach numbers give subsonic flow (Mach 0.4-0.6) into the combustor and become more oblique in higher speed flight so that the inlet flow to the combustor is supersonic (Mach 1.2-1.4). A required condition is to check that the thermal choking condition during subsonic operation does not limit the maximum temperature so much that not enough thrust can be generated. Considerations must be made given that, under supersonic combustor operation, the flow is certainly choked and the flow enters the nozzle/afterbody section at Mach = 1. Not only does this mode allow for takeoff from static conditions with the capability to reach hypersonic speeds, including Mach 8, but also reduces the inlet/engine unstarts, therefore being much more reliable since it can handle this transition.

Given the preferred approach of using a turbojet coupled with a dual-mode scramjet, the analysis options must be weighed. In this particular case there are two main options for analysis tools: Numerical Propulsion System Simulation (NPSS) and the development of custom tools. Both tools are used in this analysis. For the turbojet model, a J85 turbojet is modeled in NPSS to propel the vehicle to just over Mach 3. However, for the scramjet model, a custom tool, developed from first principles, is used over NPSS. This is the preferred approach for the scramjet model since NPSS does not have built-in libraries to account for fuel-air mixing, pre-combustion shock train, and dissociation losses across the shock waves in the inlet.

#### **D. Aerodynamics Analysis**

The objective of the aerodynamics discipline is to tie the geometry and flight conditions to the aerodynamic forces and local heating produced by the vehicle. To interface with the trajectory portion of the environment, the aerodynamics module needs to be capable of computing lift and drag at various flight conditions. Additionally, there is a thermal impact of aerodynamics due to the hypersonic flight conditions. To interface with the thermal protection module, the aerodynamics code needs to calculate surface velocity, coefficient of friction, heat transfer coefficient, and the velocity and density inside the shock wave. To perform the aerodynamic analysis of a reusable hypersonic vehicle, the analysis must be broken down into the subsonic, supersonic, and hypersonic flow regimes.

Before diving into the specific analyses of each regime, it is important to weigh the analysis options. For subsonic flow, open source options such as MIT's Athena Vortex Lattice (AVL) are available and well known in industry. However, solving for supersonic and hypersonic flow with any given geometry is exceeding difficult without the access to ITAR or

Export Controlled tools. Traditionally, NASA's CBAERO would be used for this analysis, however it is export controlled. Thus, the alternatives must be assessed. Computational Fluid Dynamics (CFD) is an option, however performing CFD correctly is both computationally and monetarily expensive. Without the time and resources to do CFD coupled with no pre-existing tools to leverage, first principles are used to approximate aerodynamic forces and heating in the supersonic and hypersonic flow regimes. These first principles take the form of tangent wedge/tangent cone analogies as well as Modified Newtonian Aerodynamics for supersonic and hypersonic flow, respectively.

### 1. Subsonic Aerodynamic Analysis

To tackle the problem of subsonic aerodynamics, MIT's Athena Vortex Lattice (AVL) is used. AVL leverages Prandtl's Lifting Line Theory where lifting surfaces are modeled as an infinitely thin sheet of discrete vortices. To visualize this, Figure 12 and Figure 13 can be used as reference [7].

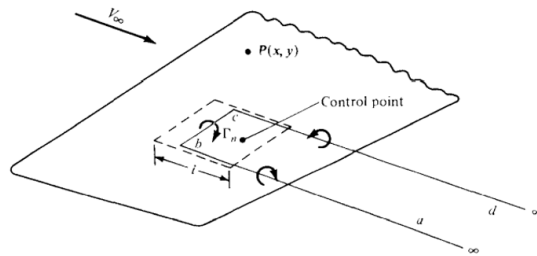


FIGURE 5.31 Schematic of a single horseshoe vortex, which is part of a vortex system on the wing.

Fig. 12 Single horseshoe vortex

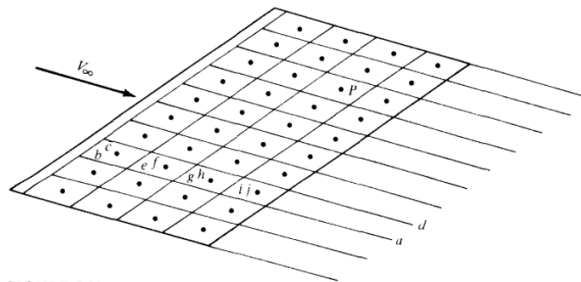


FIGURE 5.32 Vortex lattice system on a finite wing.

Fig. 13 Vortex lattice on lifting surfaces

Given the vorticity, Kutta-Joukowski Theorem can be used to calculate lift as the product of density, velocity, and circulation. The downfalls of using AVL are the same downfalls of Lifting Line Theory: the flow is assumed to be inviscid and incompressible and vortex sheets are assumed to extend to an initial rollup vortex. Additionally, this method is only applicable in the subsonic flow regime and does not account for parasitic or wave drag, only induced drag. However, AVL proves to be an accurate analysis tool and is ideal for the first-order approximations needed for this

analysis.

## 2. Geometry Interpretation

While subsonic analysis can be performed using open source software, supersonic and hypersonic analysis require the use of first principles. However, before the first principles can be applied, the geometry of the vehicle must be interpreted. To interpret the geometry for analysis, the outward normal vector must be found at each discretized cell of the mesh using the cross product as shown in Figure 14.

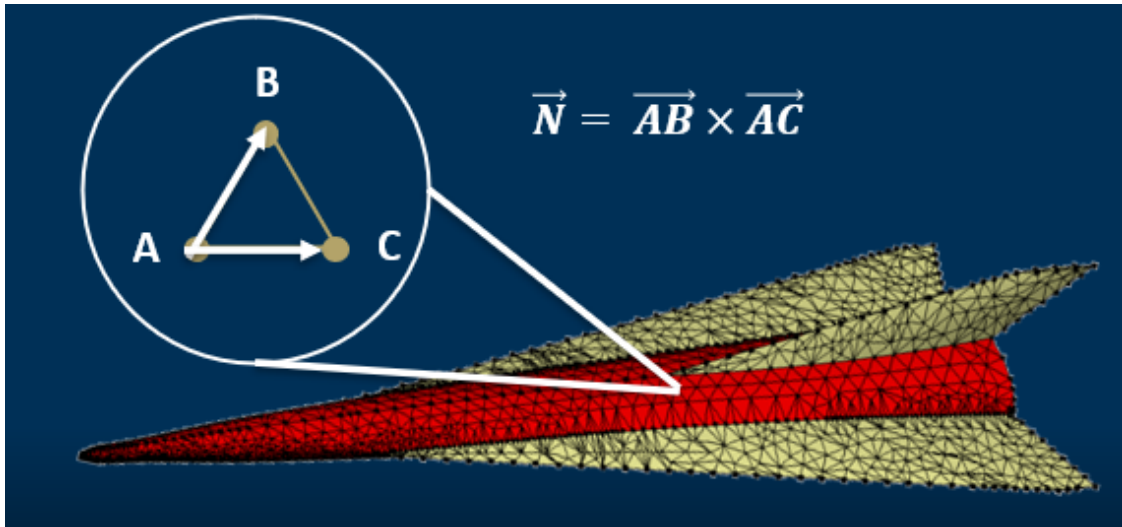


**Fig. 14** Vehicle triangular mesh

In performing the cross product, the coordinates of the vertices can be used to create two vectors that represent two edges that feed out of a single vertex. The orientation of these vectors ensures that the normal vectors are outward facing. Mathematically, if the two vectors stem away from one vertex, the cross product is outward; however, if the two vectors are oriented towards a single vertex, the cross product is inward. Following the definitions of the cross product, the outward surface normal vector can be found. This process is repeated with every cell until all surface normal vectors are found. These vectors are essential to calculate pressure using first principles.

## 3. Supersonic Aerodynamic Analysis

Without access to CFD or ITAR controlled tools, first principles are used to complete supersonic aerodynamic analysis. The first principles used in this analysis take the form of the tangent wedge/tangent cone method. The tangent wedge/tangent cone method is simply an approximation technique that proves to be accurate. In other words, there is not theory or governing principles behind the method. To visualize how tangent wedge/tangent cone approximations are performed, Figure 15 [8].

As shown in the figure, at each point "i" (which represents a cell in the vehicle mesh), a tangent line can be drawn



conditions are determined by the DoE case. After finding  $C_f$ , the heat transfer coefficient can be found next through Reynolds Analogy [8]. The Reynolds Analogy is used to relate the momentum of the flow to the heat transfer. With the Reynolds Analogy, the expression for the heat transfer coefficient can be shown below.

$$C_h = \frac{C_f \rho V C_p}{2} \quad (3)$$

The local heating analysis is fed into thermal production to select materials of interest as well as identify locations for a possible RF antenna. This local heating process is also performed for the hypersonic analysis.

#### 4. Hypersonic Aerodynamic Analysis

The first principle analysis used for hypersonics is Modified Newtonian Aerodynamics. In Newtonian Aerodynamics, when a particle contacts a surface, all the momentum normal to the surface is lost while all the momentum tangential to the surface is conserved. With this theory, the pressure the fluid exerts is assumed to originate only from the momentum lost normal to the surface. From here, the pressure coefficient at any point on the vehicle can be greatly simplified into a function of the angle of inclination of the surface and freestream velocity. Additionally, if the surface is not directly exposed to the fluid, the pressure is assumed to be equivalent to the freestream pressure which does not impact the surface. A visual of this can be shown in Figure 16 [8].

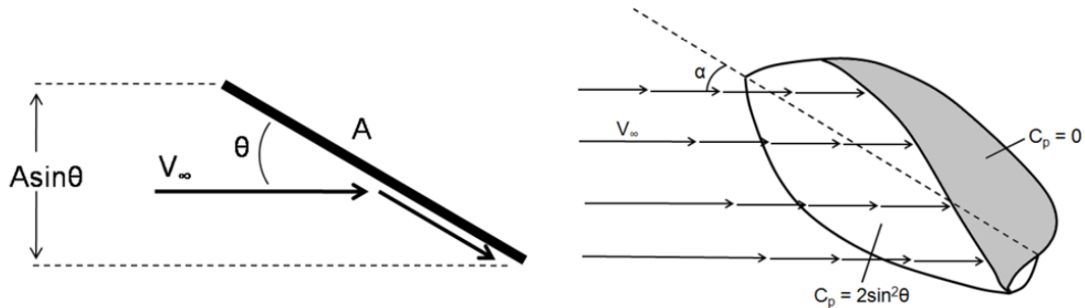


**Fig. 16 Modified Newtonian aerodynamics**

$$C_p = \frac{p - p_\infty}{\frac{1}{2} \rho_\infty V_\infty^2} = 2 \sin^2 \theta \quad (4)$$

Equation 4 displays the computation of the pressure coefficient in traditional Newtonian aerodynamic theory. However, in Modified Newtonian theory, the leading coefficient "2" is modified to account for more specific flow conditions and pressure loss across the normal shock wave. For air, this value comes out to approximately 1.81.

While Modified Newtonian theory seems simple computationally, it is far from simple to implement. In order to successfully implement this method, the geometry of the vehicle must be interpreted from a mesh in order to find the

local surface normal vectors, which are discussed the the "Geometry Interpretation" section.

With the surface normals, the angle can be calculated between the surface normal vector and the freestream, which is assumed as the x-axis. In using this angle as opposed to the angle of inclination, the  $C_p$  equation takes a slightly different form as displayed in Figure 17 and Equation 5 [9].

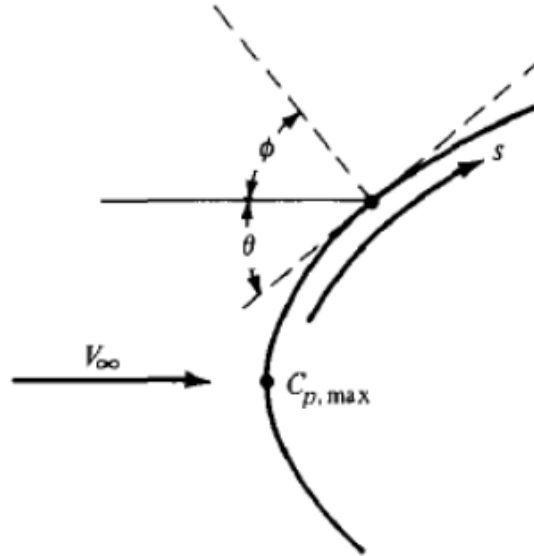


**Fig. 17 Modified Newtonian angle distinction**

$$C_p = 2\cos^2\phi \quad (5)$$

Having measured the angle between the surface normals and freestream, the pressure coefficient can be calculated at each cell. Furthermore, the pressure coefficient of each cell at a range of angles of attack can be found by changing the orientation of the x-axis. With the pressure coefficients of each cell at each angle of attack, the  $C_p$  values can be integrated over the entire vehicle to compute lift and drag coefficients, Figure 18.

Similar to the supersonic regime, the analysis does not stop here. Aerothermal heating is a key characteristic to hypersonic flight that must be accounted for. The approach to solving aerothermal heating is identical to that of the supersonic analysis however the hypersonic calculations have different values for Reynolds Number,  $C_p$ ,  $C_f$ , density, and velocity.

Having calculated the needed values, it is critical to validate the accuracy of the first principles used. To do this, a simple shape of known behaviour can be used to prove the validity of the tool. In this particular case, results of the Modified Newtonian logic can be compared to known results of a cube at zero angle of attack in hypersonic flow. In theory, the pressure coefficient of a cube in hypersonic flow is zero everywhere except the surface facing the flow which

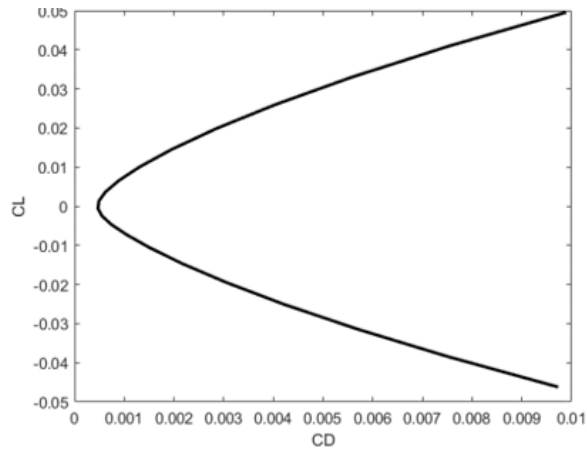


**Fig. 18 Drag polar: mach 5 at 80,000 ft**

should be approximately 2. Additionally, the coefficient of friction in the x-direction should be zero on the front and back faces and nonzero on the side surfaces. The figures below can be used to compare theory to practice.

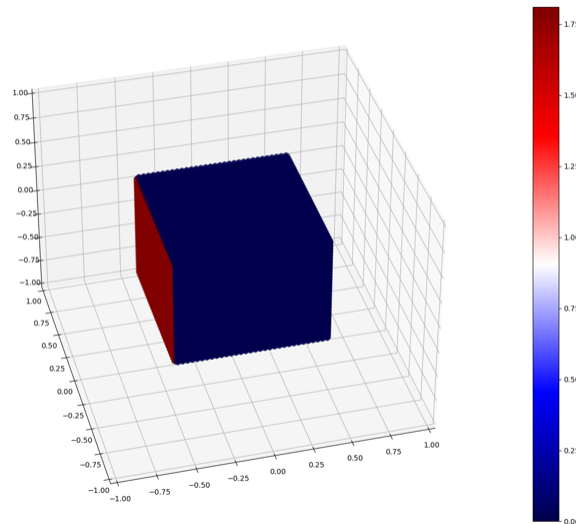


**Fig. 19 Pressure contour on a cube**

As shown in the figures, the Modified Newtonian method performs nearly identical to theory with a simple geometry and can further be analyzed on more complex geometries. While actual pressure coefficient data for the geometry shown is unavailable, the trends can be assessed for realism.

As can be seen in the Figure 21, at positive angles of attack the top surface is shadowed by the leading edge of the vehicle. The Modified Newtonian method suggests that all cells in the shadow region have  $C_p$  values of 0, which is what is seen. The same behavior can also be seen with the lower surface at negative angles of attack. While the accuracy of the  $C_p$  values for this complex geometry are unknown, the Modified Newtonian logic proves to have legitimacy in its



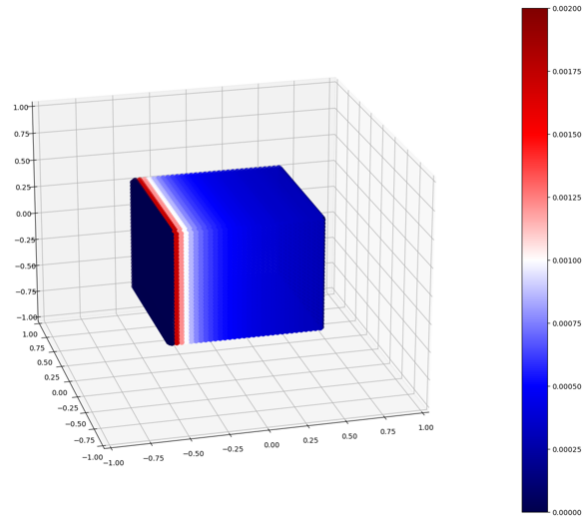


**Fig. 20 Coefficient of friction in x-direction contour on a cube**

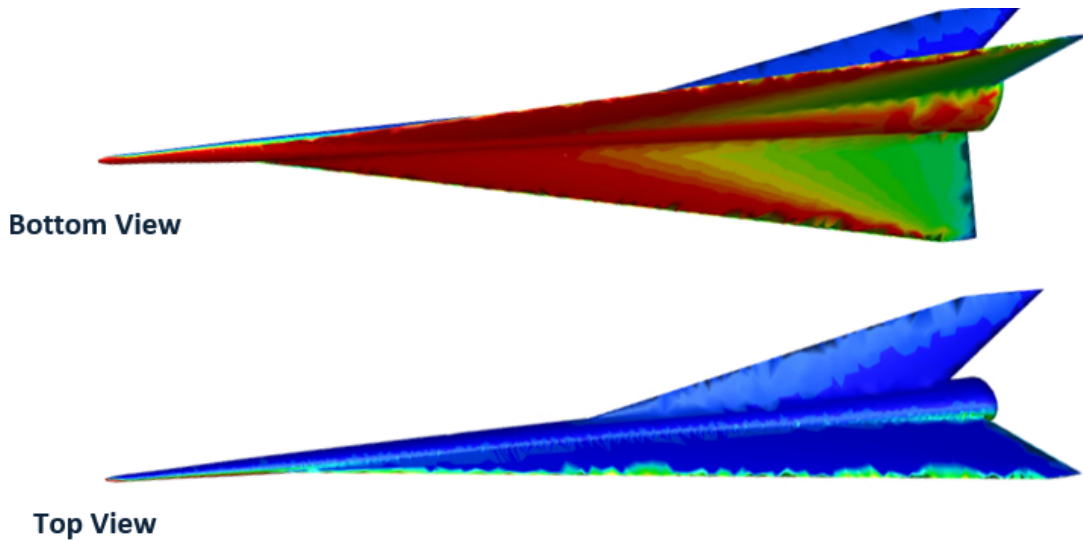


**Fig. 21 Pressure contours with positive angle of attack**

trends.

Along with pressure, the trends of the local heating can be assessed as well. Figure 22 shows a contour for the heat transfer coefficient.

As can be seen in Figure 22, the trends for the heat transfer coefficient appear correct. At zero degrees angle of attack, the leading edges show excessive heating, which is what occurs in reality.

Unfortunately, true validation of first principles models is nearly impossible without access to higher fidelity tools or ITAR/Export Controlled material. Thus, for this competition, validation can realistically only be performed on simple shapes with the analysis of trends for more complex geometries.

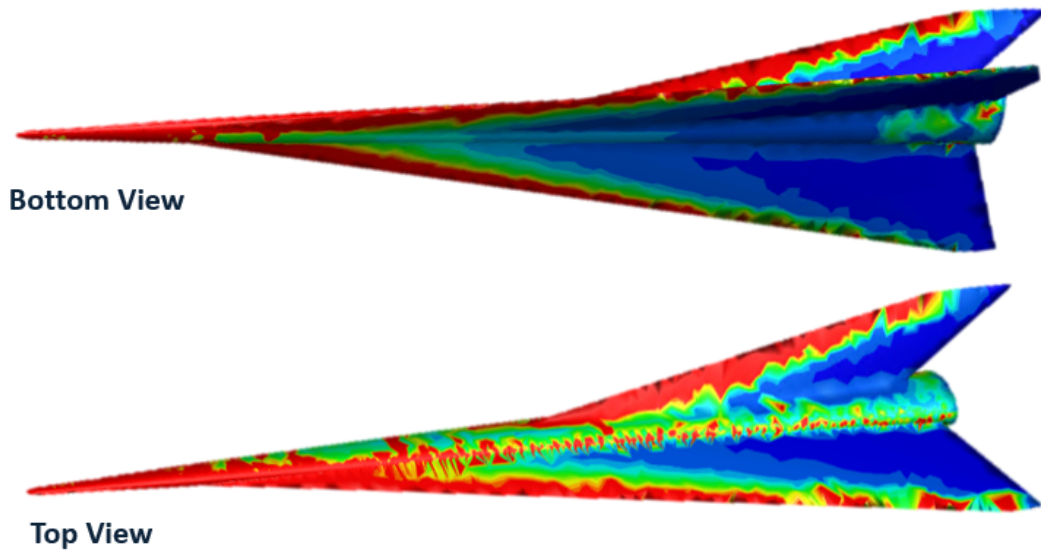


**Fig. 22 Heat transfer coefficient contour: 0 degrees angle of attack**

### E. Mission Analysis

The main objective for designing an aircraft is to successfully perform a mission. This process, however, involves many considerations that can be as simple as the aircraft's ability to fly, or as complex as the aircraft's performance when maneuvering at different flying conditions. In general, an aircraft is most efficient when flying at the conditions that drove its design (i.e., Mach number and altitude at the cruise phase for ISR platforms). Hence, most designs often underperform for the remainder of the flight profile usually due to burning more fuel with respect to the covered ground when climbing or gliding slowly while maximizing range for landing approach. Ideally, either the majority of the flying time must be spent during the design condition (cruise phase as this vehicle requires), or, in case of a complex mission profile, the aircraft must be designed with robustness in mind. The latter involves a trade between performance and efficiency in order to achieve the robustness required to perform relatively well in most aspects, something that is not well suited for the design of a hypersonic ISR platform with the objective of gathering information as fast as possible without excessive maneuvering. Therefore, the UPRISE design will be mostly driven by the cruise phase, with additional considerations for the climb and descent phases. Since the UPRISE vehicle must be capable of one-way and round-trip missions, knowing that the most constrained flying conditions are encountered during the high-speed turning phase, the aircraft is designed to withstand up to a maximum load factor of  $2g$ . This enables both types of mission profiles with a relatively low increase in the gross weight of the aircraft.

Considering that the rigid-body attitude motions of the aircraft occur very rapidly (e.g., in the order of seconds) and that the time to climb is most likely in the order of minutes, the motion of the aircraft can be approximated as quasi-instantaneous [10], meaning that the aircraft can be treated as a point mass, where the moments and forces

acting on the aircraft are considered to act on the center of mass as illustrated on Figure 23. Considering pseudo two

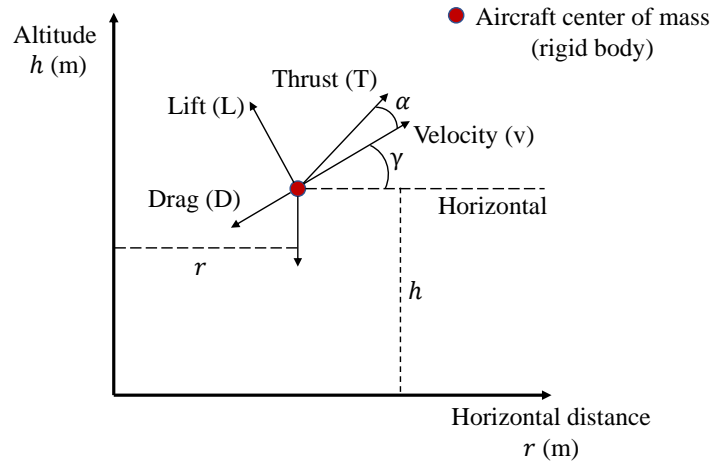


**Fig. 23 Free body diagram of the aircraft modeled as a point mass**

dimensional motion, the aircraft is governed by the following dynamic constraints:

$$\frac{dv}{dt} = \frac{T}{m} \cos \alpha - \frac{D}{m} - g \sin \gamma \quad (6)$$

$$\frac{d\gamma}{dt} = \frac{T}{mv} \sin \alpha + \frac{L}{mv} - \frac{g \cos \gamma}{v} \quad (7)$$

$$\frac{dh}{dt} = v \sin \gamma \quad (8)$$

$$\frac{dr}{dt} = v \cos \gamma \quad (9)$$

$$\frac{dm}{dt} = -\frac{T}{gI_{sp}} \quad (10)$$

Equation 6 describes the rate of change of velocity of the aircraft (i.e., its acceleration). This depends on the amount of thrust that the engine can produce per unit mass in the direction of the local velocity flow (given by the angle of attack) and is affected by both the amount of drag per unit mass and the aircraft orientation given by the flight path angle. This means that a lighter aircraft will accelerate faster compared to a heavier aircraft, provided that both have the same engine and aerodynamic properties. Note that for any given aircraft concept, the acceleration is maximized when both the angle of attack and the flight path angle are zero. Equation 7 describes the rate of change of the flight path angle (i.e., the angle between the horizontal and the velocity vector). This describes whether the aircraft is climbing or descending (positive or negative  $\gamma$  means ascending or descending respectively). For steady-level flight, the flight path angle would be zero. Also, notice that the angle of attack is used as the control variable to control the orientation of the aircraft. Equation 8 describes the rate of change of the altitude of the aircraft. For a given aircraft speed, since the flight

path angle is measured from the horizontal, the closer that this angle is to  $90^\circ$ , the faster that the aircraft will climb. However, having a maximum flight path angle might not be the best choice as the thrust produced by the engine must overcome the weight of the aircraft in order to climb. Also, large values for  $\gamma$  are detrimental to the acceleration of the aircraft as described by Equation 8. There is also a competing effect between Equation 8 and the rate of the distance that the aircraft covers with respect to the ground (i.e., the range) described by Equation 9 due to requiring opposite optimization of the flight path angle. This is because, for a given aircraft speed, a minimum flight path angle represents the maximum rate of change in range and a maximum flight path angle represents the maximum rate of change in altitude. Equation 10 describes the rate of change of the gross weight of the aircraft as fuel is being burned. This is heavily dependent on the engine design parameters (e.g., thrust, specific impulse). For a given value of atmospheric density, an engine with a higher specific impulse is more efficient because it produces more thrust while using the same amount of fuel. Therefore, the fuel consumption over time will only depend on the thrust produced by the engine (assuming the force of gravity per unit mass is constant). Calculating the weight of the aircraft at any instance of time is important because it will determine the amount of lift that the aircraft needs to produce. Equation 6 to 10 govern the dynamics of the aircraft as they represent the equations of motion.

The following subsections give a detailed description of the modeling approach for the multiple phases of our mission profile: 1) takeoff and climb using maximum thrust to reach the desired cruise condition as quick as possible, 2) cruise at the design condition for the maximum range, and 3) descent and landing approach considering the required runway length. The modeling of the climb phase is done through Dymos, a platform that allows for the simulation and optimization of the trajectory for a given condition.

### 1. Takeoff and Climb

Ideally, the UPRISE vehicle must achieve the desired cruising altitude and speed in the minimum amount of time. This process however is not trivial due to sudden changes in the flight conditions and the variation in performance of the aircraft along the flight path. This problem can be modeled as a constrained optimization problem, where the objective is to minimize the functional time that it takes to reach the desired altitude and speed. This expression of this objective is shown below.

$$\min J = t_f \tag{11}$$

Subject to the initial boundary conditions:

$$r_0 = 0 \text{ m}, h_0 = 100 \text{ m}, v_0 = 0 \text{ m/s}, \gamma_0 = 0^\circ, \text{ and } m_0 = W_{gross}, \tag{12}$$

And the final boundary conditions:

$$h_f \geq 80000 \text{ ft}, M_f \geq 5, \gamma_f = 0^\circ. \tag{13}$$

The final boundary conditions depend on the aircraft design conditions presented later in Section VI.A. Also, given that the RFP does not specify a takeoff runway length, the team assumed that the maximum takeoff runway length is equal to the maximum landing runway length (e.g., 8000 ft). In this case, a constraint is introduced so that the aircraft remains on the ground until it produces enough lift to overcome the  $W_{gross}$ , and this must be done before covering a ground distance of 8000 ft. Notice that the team does not consider clearing an obstacle for this problem, hence the aircraft is free to climb at any rate it can support. Notice that the boundary conditions from Equation 12 and 13 show that the aircraft should start and end on a steady-level flight condition. For the climb phase, since the range is not specified or considered as a boundary condition, Eq. 10 can be ignored, leaving altitude, speed, and flight path angle as the optimization variables of focus.

The climb phase is particularly difficult for two main reasons: 1) the aircraft must fly through four different flow regimes: subsonic, transonic, supersonic, and hypersonic, and 2) considerations must be made for the varying performance of the two different propulsion systems and the transition between their usage.

The aerodynamic performance of the aircraft depends on the aircraft's speed and altitude within the mission profile. The aircraft encounters the most amount of drag during the transition from the subsonic to the transonic regimes, and later from the transonic to the supersonic regimes, where the large difference in pressure gradients between subsonic and supersonic flows drive a large amount of drag on the aircraft. A maneuver often done to overcome this effect is to quickly dive to pass through the transonic regime as fast as possible. How the UPRISE aircraft behaves during this transition is discussed later in the results section. On the other hand, the aerodynamic effects resulting from the transition between the supersonic and hypersonic flows in the form of instability waves in the boundary layer is ignored due to its complexity to model from first principles approaches.

Similar to aerodynamics, the propulsion performance also changes with changing altitude and speed. Since the modified J85 model is valid for  $M \leq 3.5$  and  $h \leq 60000$  ft, the turbojet is used to accelerate the UPRISE vehicle until these conditions are reached. At this point, the inlet of the turbojet flow path is covered and the inlet to the dual-mode scramjet flow path is opened, and the latter engine takes over. Notice that at any point during the mission, the corresponding active engine must produce enough thrust to overcome or balance the drag forces, so that enough lift is produced to overcome or balance the weight of the aircraft.

## 2. Hypersonic Cruise and High-Speed Turning Flight

Once the aircraft has reached the design altitude and speed, the cruise phase begins. For simplicity and computational speed, this phase is not simulated using Dymos, instead, a segmented Breguet Range approach is implemented as described by the equation below.

$$r = v \times \frac{L}{D} \times I_{sp} \times \ln \frac{W_0}{W_f} \quad (14)$$

with this approach, the entire phase is discretized into small linear segments (note: a sensitivity study shows that  $10^2$  segments are enough for high accuracy, e.g, less than 1% relative error). At the end of each segment, the aircraft cruise conditions such as its covered ground distance, fuel burn, thrust required, and current mass are calculated. These values determine the initial conditions for the next segment, and their cumulative sum is recorded over time to determine the ability of the aircraft to perform the mission successfully (e.g., if the aircraft has enough fuel and thrust for a given range). The reason for this segmented approach is related to the decrease in weight of the vehicle over time as fuel burns. At each point in the cruise segment, given that the conditions for steady level flight (e.g.,  $\frac{dv}{dt} = 0$ ) are such that the lift must balance the weight and the thrust must balance the drag, as the weight changes, so does the required L/D. This requires the aircraft to adjust its angle of attack over time to fly at the same altitude and speed for the duration of the cruise segment. Since the range covering these segments is very small (relating to almost instantaneous dynamic changes), the entire cruise phase is effectively dynamically continuous. A similar approach is used for the round-trip mission where the cruise condition is mostly dominated ( $\sim 95\%$  of the cruise) by a high-speed turning flight. This is because the loads on the aircraft rapidly increase when turning at a high speed, and in order to minimize the loads, the turning angle must be reduced. This increases the turning radius and consequently the ground distance covered. Since the objective is to return to the takeoff place, it is convenient to design the aircraft considering the more constrained requirements of the high-speed turning phase. This is because an aircraft that can perform a round-trip can not only maneuver but also fulfill the one-way mission as well. Therefore, this turning phase mostly dominates the design of the aircraft since it is the most demanding, with the penalty of requiring an aircraft almost three times as heavy as one that might be designed for a simple one-way mission. Therefore, the structural, mechanical, and propulsive designs are scaled in a way such that they only depend on whether the aircraft can fly a round-trip mission supporting up to a  $2g$  load or not.

### 3. *Descent and Landing*

At the end of the cruise segment, the scramjet is shut down and the aircraft starts to glide towards the final destination. This can be solved by modifying the optimization problem from the climb phase by reverting the boundary conditions and setting the maximum thrust to zero. However, in this case, the goal is to maximize the ground distance covered while gliding, as well as constraining the speed so that the aircraft does not stall. This can be expressed by the following equation.

$$v_{stall} = \sqrt{\frac{2W}{\rho S C_{L,max}}}. \quad (15)$$

Since the requirement for a landing runway length must be a design consideration, the aircraft must have wings large enough to produce enough lift at low speeds such that it can land at less than 8000 ft, but also small enough to produce the least amount of drag when cruising. The first condition can be accounted for as a constraint in the design and

selection of the latter will be discussed later in section VI.

## F. Thermal Protection Analysis

Based on requirements stated in the RFP, the sized vehicle is designed to operate between flight speeds of Mach 5 and 8 and between altitudes of 80,000 to 100,000 ft. Since the RFP prohibits the usage of any ITAR/export controlled tools, it is prohibited to use tools such as TPSSizer for the analysis of the thermal protection system. In addition, the vehicle has a strict reusability requirement of less than 24 hours of turn around time between sorties. This requirement especially poses challenges to the thermal design process since most common thermal protection materials are ablative and designed for a single use on re-entry vehicles. Due to the chemical nature of ablative thermal protection materials, the tiles undergo pyrolysis during re-entry portion of the flight, essentially burning off a portion of the thermal protection layer. This chemical reaction protects the important components and instruments from burning up during re-entry, but it also causes permanent wear on the thermal protection material. Therefore, it takes a long time between missions to repair and overhaul, often times requiring several months to replace the thermal protection tiles completely. In order to fulfill the competition design requirements, research is focus on ceramic and metallic based non-ablative thermal protection materials. Active thermal protection systems are considered, but comparing to the passive TPS options, they are still in early development. Active TPS options are also relatively heavy compared to the passive options since they often involve complex coolant circulation mechanisms.

In order to make the correct TPS selection without the use of any restricted tools, a first principles approach is used to perform the thermal analysis. The analysis starts with estimating the heat flux and temperature at the nose of the vehicle since this is one of the hottest regions on the vehicle during flight. Based on the vehicle preliminary sizing modules, the nose radius of the vehicle is determined. With the nose radius and the associated flight regime, the Sutton-Graves model is used to account for convection and the Tauber-Sutton model is used to account for radiation. As shown in the formula below,  $c$ ,  $a$ ,  $b$ , and  $f(v)$  are tabulated data.

Since there is a normal shock generated in front of the nose of the vehicle, isentropic shock equations are used to get the conditions downstream of the shock. The isentropic shock equations are a function of the post normal shock density, velocity of the vehicle, nose radius, and emissivity. In terms of the output, the heat flux and wall temperature are calculated as expressed below.

$$q_{convective} = (k) \cdot \sqrt{\frac{\rho}{R_{nose}}} \cdot v^3, k_{earth} = 1.7415 \times 10^{-4} \quad (16)$$

$$q_{radiative} = CR_n^a \rho_\infty^b f(v) \quad (17)$$

After performing the necessary calculations, potential TPS potentials can be assessed. Shown in Figure 24, the

thermal performance of several different TPS options are plotted with respect to the flight altitude and Mach number. The green highlighted region shows the cruise regime of the UPRISE vehicle as derived from the competition RFP. Under the assumed nose radius, Ultra High Temperature Ceramics (UHTC) are the most suitable material for this application. Based on the analysis, UHTC materials are suitable for flight conditions throughout the entire mission profile.

It is important to remember the coupled nature of hypersonic aircraft design. Depending on the selected TPS material, multiple considerations must be made, such as material weight, cost, etc., that must feed forward and backgrounds in the design environment. However, for the simplicity of this analysis, only the weight and cost of the TPS material are considered in the design environment. Other factors such as ductility, tensile strength, etc. are omitted from this analysis.

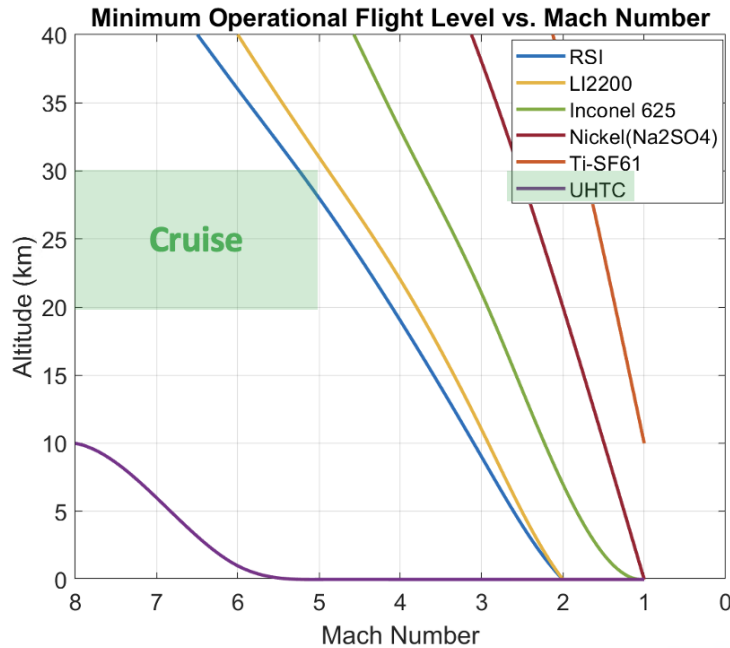


**Fig. 24 TPS material feasible space**

### G. Cost Analysis

The cost analysis is used to create estimates for different aspects of the program such as maintenance, operating, and vehicle costs. By developing cost models and accounting for them in the design environment, the cost is considered in the design process. There are multiple methods available for accurately generating costs estimates. The first option would be a methods engineering or a bottoms-up approach. This method involves very detailed analysis of individual components of everything leading into the final costs and then summing them all together. This method requires a very good understanding of the design in order to accurately come up with component costs. Next, there is the analogy



method where particular costs are gathered from past programs with complexity factors applied for the design at hand. This method is based off of realistic values but the complexity factors can be difficult to accurately create and may require extensive efforts to develop. Finally, there is the statistical regression technique which is commonly one of the best tools to use early in the design stage. These equations are generated based solely on similar aircraft whose characteristics are known. For many aspects of costs, there has been shown to be fairly accurate relationships between cost and vehicle parameters such as weight or thrust.

Additionally, in order to find the most accurate cost estimates, the challenges associated with this task need to be understood. Given the current state of hypersonic vehicles, particularly for reusable and air-breathing aircraft, there is very limited public information on cost estimates. This is due to multiple factors but none as influential as the fact that this type of vehicle has never existed. In commercial aviation, for example, there are many past as well as derivative aircraft to compare with. Even for supersonic military jets, there are previous generations to refer to. For the particular vehicle required in this competition, there are essentially no comparable vehicles with similar technologies. This makes it impossible to generate regressions off of past aircraft. Building onto this, any information that may be available is definitely not available to the public given that hypersonic technology is very sensitive information in regards to national defense. Therefore, a great deal of information that could be helpful in a cost estimate is likely to be labeled as classified information. The next challenge concerns the fact that much of the technology, such as materials and hypersonic propulsion systems, are still being developed. Because of this, many costs that currently exist could change and greatly increase as research, development, and testing continues. Finally, and most generic to any conceptual level design, there are just too many unknowns at this stage to be able to completely and accurately create a cost estimate. While this is always the case, the uncertainties that play into the estimates will be much larger for the hypersonic platform due to the additional factors previously mentioned.

After researching cost methods and searching for resources on the topic, the cost estimates that are described below make use of analogy and statistical regression techniques. Several cost estimates are generated purely from calculations or literature research. This would include considerations like the price of fuel since the amount of fuel can just be multiplied by the cost. For certain components of the cost analysis, there is little to no change with respect to different aircraft types or technologies. For these cases, regressions can be utilized. For more difficult estimates, a combination of analogy and regression techniques are used for the UPRISE vehicle.

### *1. Maintenance Cost*

The entirety of the maintenance costs come from a NASA contractor report on hypersonic transports [11]. This set of equations are for hypersonic aircraft for commercial aviation. While the vehicle in this competition is for military use, the technology to accomplish reusable hypersonic flight would be similar, yielding appropriate equations for maintenance costs. The maintenance costs are divided between the airframe, turbojet, and scramjet. Within each of

these divisions, they are further categorized by the material cost and labor cost. For the UPRISE design, the differences in maintenance labor and materials are deemed to be insignificant.

$$maintenance_{af,l} = \frac{(2 + 1.2t_f)[0.05(\frac{W_{af}}{W_{gto}} + \frac{W_{av}}{W_{gto}} + coef)M_c^5(r_l)]}{\frac{W_{pl}}{W_{gto}}R} \quad (18)$$

$$coef = (\frac{6}{W_{gto}} - \frac{360}{(\frac{W_{af}+W_{av}}{1000} + 120)W_{gto}}) \cdot 10^3 \quad (19)$$

$$maintenance_{af,m} = \frac{(12.4 + 6.2t_f)(\frac{C_{vehicle}-C_{tj}-C_{rj}}{W_{gto}})}{\frac{W_{pl}}{W_{gto}}R \cdot 1000} \quad (20)$$

$$maintenance_{tj,l} = \frac{(\frac{T}{W})_{gto}(1 + 0.3t_f)(\frac{1.2}{T_{tj} \cdot 10^3} + 0.054)r_l K_{ltj}}{\frac{W_{pl}}{W_{gto}}R} \quad (21)$$

$$maintenance_{tj,m} = \frac{(\frac{C_{tj}}{W_{gto}})(0.04 + 0.015t_f)K_{mtj}}{\frac{W_{pl}}{W_{gto}}R} \quad (22)$$

$$maintenance_{sj,l} = \frac{(1 + t_f)(\frac{0.876N_{sj}(\frac{L}{D})}{W_{gto}/10^3} + 0.087)r_l K_{lsj}}{\frac{L}{D} \frac{W_{pl}}{W_{gto}}R} \quad (23)$$

$$maintenance_{sj,m} = \frac{(\frac{C_{tj}}{W_{gto}})(0.029 + 0.036t_f)K_{msj}}{\frac{W_{pl}}{W_{gto}}R} \quad (24)$$

From the above equations the breakdown of maintenance cost can be determined with the entirety of the maintenance cost being the summation of the six equations. The estimates are in units of cent/ton-mile in 1972 dollars. The values presented later are converted to 2022 dollars.

Many of the variables in the maintenance equations are values that are found in the vehicle analysis. These values include: time of flight, vehicle weights, cruise Mach number, thrust to weight ratio, and the number of turbojets. These are inputs into the cost equations within the design environment and are used to calculate the costs for each unique vehicle. The other variables in the equations are either assumptions or assigned a constant value based on literature. The labor rate ( $r_l$ ) is assigned based on the value used in the NASA hypersonic report [11]. The value was \$5.30 per hour in the year 1967. However since the equations are calculated for 1972, the value used in the equations is \$6.63 per hour to account for inflation. Then, the range (R) is assigned to be 3000 nmi but had to be converted to miles by multiplying this by 1.15. The range is the objective range as outlined in the RFP [1]. Next are the cost values of the vehicle, the turbojet, and scramjet. The vehicle cost is determined in Equation 27. The turbojet is assumed to be \$32 million based on the

price of a F135 turbojet engine [12]. Next the cost of a scramjet engine was assumed to be \$50 million. This value could not be exactly found and is based on estimated development costs. According to a 2003 estimate for the National Hypersonics Initiative, development costs for both turbojet and scramjet engines for a hypersonic vehicle would be between \$8-\$14 billion [13]. Based proportionally on F135 program costs, the scramjet is assumed to be \$50 million. Finally, the K values, which are ratios for the engines, are all assigned values according to the NASA hypersonic report [11]. The values for  $K_{ltj}$ ,  $K_{mtj}$ ,  $K_{lsj}$ , and  $K_{msj}$  are 2, 2, 2, and 3 respectively.

## 2. Operating Cost

The total operating cost is the accumulation of multiple different components. It is the summation of fuel, maintenance, depreciation, and overhead costs all on a per mission basis. While fuel cost is calculated in literature on a per mission basis, maintenance, depreciation, and overhead costs must be recalculated to account for operating costs per mission. The fuel cost is calculated by taking the total weight of fuel and multiplying that by the cost of fuel. The cost of fuel used is 3.85 dollars per gallon for Jet-A fuel [14]. The maintenance costs are the values as outlined previously. As these values are cents per ton-mile, the takeoff weight and distance travelled per mission is used to calculate the maintenance costs per mission. The next value considered in the operating cost is the depreciation of the vehicle. The equation is shown below:

$$C_{depreciation} = \frac{1.1\left(\frac{C_{unit}}{W_{gto}}\right) + 0.3\left(\frac{C_{tj} + C_{sj}}{W_{gto}}\right)}{0.34 \frac{W_{pl}}{W_{gto}} M_c \frac{V_b}{V_{cr}} UL_d} \quad (25)$$

This estimate is from the same report as the maintenance equations [11]. Similarly, the units are in cents/ton-mile and are changed to accommodate for a per mission estimate in 2022 dollars.

The final component of the operating cost is the overhead costs. The overhead is determined as a percentage of the other operating costs. From an ICAO report, it is stated that overhead is about 13% of total operating costs [15]. This estimate is for commercial airlines with a percent assigned to marketing. Since this would not be a consideration for a military aircraft, the percentage was recalculated to represent the same amount. With this logic, the overhead cost was estimated using the following equation.

$$C_{overhead} = (C_{fuel} + C_{maintenance} + C_{depreciation}) \cdot 0.22 \quad (26)$$

## 3. Vehicle Cost

The acquisition cost of the vehicle is a function of many different factors. The first consideration is the actual cost of making a single aircraft. Once this value is determined, other costs that are incurred for the production of the vehicle must be factored into the final selling price. These values are the cost of RDT&E and tooling.

The vehicle cost is based on a NASA market study about a generic hypersonic airliner [16]. This report provides holistic studies on the market for commercial hypersonic transportation. One section of the report provides cost estimates for different aircraft based on cruise speed, payload, and propulsion system. For generating the vehicle cost in this program, a simple regression equation is generated using these estimates to provide an equation as a function of Mach number and payload. This equation is summarized in Equation 27 below.

$$C_{unit} = (90 \cdot M_c + 0.00125 \cdot W_{pl}) \cdot 10^6 \quad (27)$$

The cost estimates for these aircraft factor in the production and tooling (materials and manufacturing), but do not consider the RDT&E costs. With the cost of producing a vehicle described, the RDT&E then should be calculated. This cost is estimated by summing the engineering, tooling, and developmental costs. Testing is considered in the engineering and development costs. The first consideration is the engineering, which makes up a substantial portion of the RDT&E cost. This value is found using Equation 28 for military airframe development from a RAND report [17]. The value for advmat (which is a percentage of advanced materials) was assumed to be 0.98 based on previous aircraft such as the SR-71 and X-15. As these values would likely require less of these materials, a higher value is assigned for the cost analysis of the vehicle in this competition. This value is selected based on an average between these aircraft and 100% of the materials. As this value did not play a large impact on the engineering cost and total costs, this assumed value is deemed acceptable. The rate of engineering is assumed to be an average of \$50/hr.

$$C_{nEng} = 7924.314 \cdot W_e^{0.561} \text{advmat}^{0.671} 1.034^f r_{eng} \quad (28)$$

There are also considerations of tooling in the same RAND report [17]. This value is the tooling cost (labor and equipment) for a particular aircraft manufacturing program. The equation first calculates the labor cost for tooling and then multiplies a factor to accommodate for the cost of equipment. The labor is from the RAND report while the addition of equipment cost is taken from a metal working website, MSC [18]. In the equation, the rate of tooling is assumed to be slightly more than the rate of maintenance from the previously mentioned NASA direct operating cost report. In the equation, the labor rate ( $r_t$ ) is assumed to be an average of \$35/hr.

$$C_{tooling} = 2769.13 \cdot W_{af}^{0.685} \text{advmat}^{0.075} \text{rate}^{0.57} r_t \cdot (58/31) \quad (29)$$

Then the RDT&E cost incorporates the developmental vehicles and controls stations outlined in the RFP. The vehicle unit cost is determined from Equation 27. The cost of the control station is based on the cost of one for the MQ-9 Reaper. The cost is found to be \$3.17 million per station [19]. Finally, the total development cost for the engines would need to be incorporated. As the turbojet would already be developed, only the scramjet would need to be developed. Based on

another NASA study, the cost of new engine development over 10 years on a military aircraft is approximately \$1 billion [20]. With all these costs outlined, the total RDT&E cost is shown in Equation 30 below.

$$C_{RDT\&E} = C_{nEng} + C_{tooling} + 5 \cdot C_{unit} + 2 \cdot C_{cs} + 10^9 \quad (30)$$

Finally, once the RDT&E costs are determined, the final cost for the entire platform can be found. The total cost of the vehicle is the combination of a single vehicle plus the entire program cost (RDT&E) spread out over the number of vehicles that are going to be produced. Per the program outline, there will be 10 aircraft produced over 10 years. This means the RDT&E costs should be divided by 100 to factor in the cost per vehicle produced. The equation for total vehicle cost is shown below in Equation 31.

$$C_{vehicle} = (C_{RDT\&E})/100 + C_{unit} \quad (31)$$

The acquisition cost of the platform would then be the total vehicle cost with the amount of profit that will be applied for the manufacturer. Based on a study of profit for the British DoD, it was determined that 15 percent is too high of a profit margin [21]. With this in mind, the reasonable profit was assumed to be 7 percent. With this assumption, the vehicle acquisition price is summarized in Equation 32.

$$C_{vehicle,aq} = C_{vehicle} \cdot 1.07 \quad (32)$$

#### 4. Miscellaneous Cost

The main cost that would be captured outside of those previously mentioned would include unique or support equipment and systems. The considerations in this category would include a mothership or rocket boosters if they were used. However, such systems are not part of the final design and therefore need not be included in the cost analysis. Since these forms of support would greatly increase the overall cost of the platform and degrade vehicle reusability, the team decided earlier in the design process to eliminate these options from the morphological matrix. The requirements also led to considering less complex and complimentary designs. While making these design decisions, the cost of the system is considered, thus requiring no additional costs for the program.

## VI. Design Space Exploration

After developing the modeling and simulation environment that comprises the multi-disciplinary integration process, different combinations of design parameters (*i.e.*, different geometrical and functional characteristics) can be explored for the UPRISE down-selected configurations. This process allows not only examines the performance of different aircraft but also obtains the optimum design considering the mission requirements. The goal of this design approach is

to systematically find a vehicle that can successfully complete the mission while maximizing the performance of the aircraft.

Performing a design space exploration allows for the understanding of the important design variables and their contribution to the final design. Additionally, this approach allows for the generation of surrogate models that enable studying the sensitivity of the design variables on the final design of the aircraft. However, before thoroughly exploring the design space, a design of experiments (DoE) must be generated to sample the seemingly infinite design space. A DoE considers a finite range for each design variable that is often selected based on the physical limits for each variable. Each DoE entry (assuming no repetition), results in a unique design. With the results from a broad DoE, a detailed analysis can be performed across the previously down selected architectures. How the design environment is constructed, if cases converge at given conditions laid out in the RFP, the vehicle is guaranteed to meet those requirements. The "baked-in" requirements from the design environment include the Mach number, altitude, and range. After running a coarse DoE, refined DoEs can be performed with more narrow regions to capture a more feasible design space. With refined DoE results, surrogates can be fit to optimize the vehicle to best meet requirements.

#### **A. DoE Inputs/Outputs**

To generate a DoE, engineering judgement had to be used to determine the ranges of the variables. Since there are no proven existing systems to base the DoE off of, aircraft that are most similar (like D-21) can be used as a guide with very large ranges to account for uncertainty. The first set of variables that can be modified are the flights conditions: Mach number, altitude, and range. These variables are set to the limits of the specified requirements. Any designs that converge with a given flight condition is sure to meet the set requirements. The next set of parameters describe the vehicle. The variables and their respective ranges can be seen below.

**Table 4 Flight conditions DoE ranges**

<b>Parameter</b>	<b>Minimum</b>	<b>Maximum</b>
Mach	5	8
Altitude(ft)	80,000	100,000
Range(nmi)	2,500	3,000

Having selected the design variables and their corresponding ranges, a comprehensive DoE can be generated using a fractional factorial approach to sample the corners and edges of the design space, and a Latin Hypercube approach to explore the interior of the design space. The fractional factorial approach is convenient because using a full factorial approach for 17 design variables yields 131072 combinations. With full factorial, assuming that the edges of the design space require approximately 20% of the total number of cases, then the total number of combinations required for this approach would be almost a million. Therefore, the fractional factorial approach effectively allows using a fraction of the required cases (~2000 in this case). The Latin Hypercube ensures that the inside of the design space is well resolved

**Table 5 Vehicle parameters DoE ranges**

<b>Parameter</b>	<b>Minimum</b>	<b>Maximum</b>
Fuselage height to width ratio	0.2	1.1
Fineness ratio	5	10
Nose radius	0.033 ft	0.33 ft
Load factor	1	2 ft
Wing Aspect ratio	0.7	1.7
Wing loading	70	110
Wing thickness to chord ratio	0.01	0.03
Wing dihedral	-10°	10°
Wing taper ratio	0.02	0.10
Wing sweep ratio	70	75
Vertical tail volume coefficient	0.04	0.065
Vertical tail aspect ratio	0.7	2.5
Vertical tail taper ratio	0.05	0.5
Vertical tail sweep	55°	75°

by providing optimal spacing between the the points within the multi-dimensional space (~8000 points selected in this case for a total of 10000 combinations). To evaluate the results, the following parameters are considered: takeoff gross weight, fuel mass fraction, thrust-to-weight ratio, specific impulse, reference wing area, stagnation wall temperature, fuselage width and diameter, maintenance direct operating cost per mission, total operating cost per mission, RDT&E cost, and unit acquisition price. Note that most of the parameters of interest are sizing and cost parameters. Each individual case in the DoE has a unique set of outputs. With each set of outputs, a statistical analysis software called JMP can be used to explore the design space. Using JMP, the outputs can first be placed in a scatterplot matrix to explore relationships between outputs as seen in Figure 25.

From here specific limits can be set on the results to isolate more feasible concepts. Given the payload weight of 1000lb, an initial assumption was made that the vehicle will likely not need to exceed 50,000lb gross weight. Applying this filter, Figure 26 displays the designs weighing less that 50,000lb.

It is important to keep in mind that these results are only for the cruise segment of the mission. Additional analyses are performed outside of the loop with the potential designs that meet cruise requirements in order to expedite run time. Due to the significant computational time of the coupled approach, surrogate modeling is needed to rapidly perform trade studies.

Before generating the surrogates, the results of the DoE can be analyzed to find the most influential factors on the outputs of interests. The goal of this screening process is to identify these important factors in order to build surrogates that connect the input parameters to the outputs of interest. This screening process can also be done using JMP. To perform the screening process, Artificial Neural Networks (ANN) are used to display and rank the parameters that are

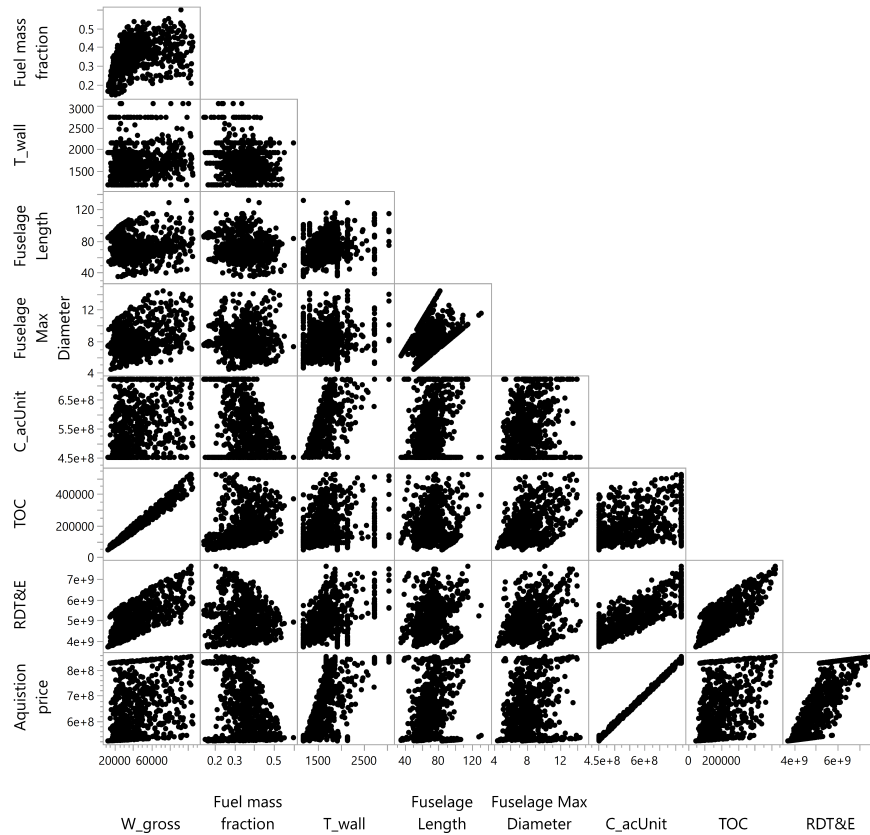


**Fig. 25 Overall scatter plot matrix**

most influential to the results.

Assessing the outputs, thrust to weight is the most significant variable for this particular set of data. This observation is logical as thrust to weight is a sizing parameter with great influence in the MDA environment.

### 1. Surrogates

After the screening is complete, surrogates can be generated. While the results of the DoE produce many feasible solutions, they may not produce the optimal solution, particularly with continuous variables involved. Surrogate models can be fit to the DoE results in order to set desirability's to identify an optimal solution that meets requirements and weighs and costs the least.

Additionally, due to the complex nature of the problem, achieving vehicle closure in the MDA environment is incredibly expensive computationally. Thus a method is needed to speed up the analysis. Surrogate models do exactly this. The purpose of surrogates are to expedite the computation time in order to perform trade studies.

To ensure the surrogate models fit the data well, surrogates can be selected based on the following criteria:

- $R^2$
- Model Representation Error (MRE)



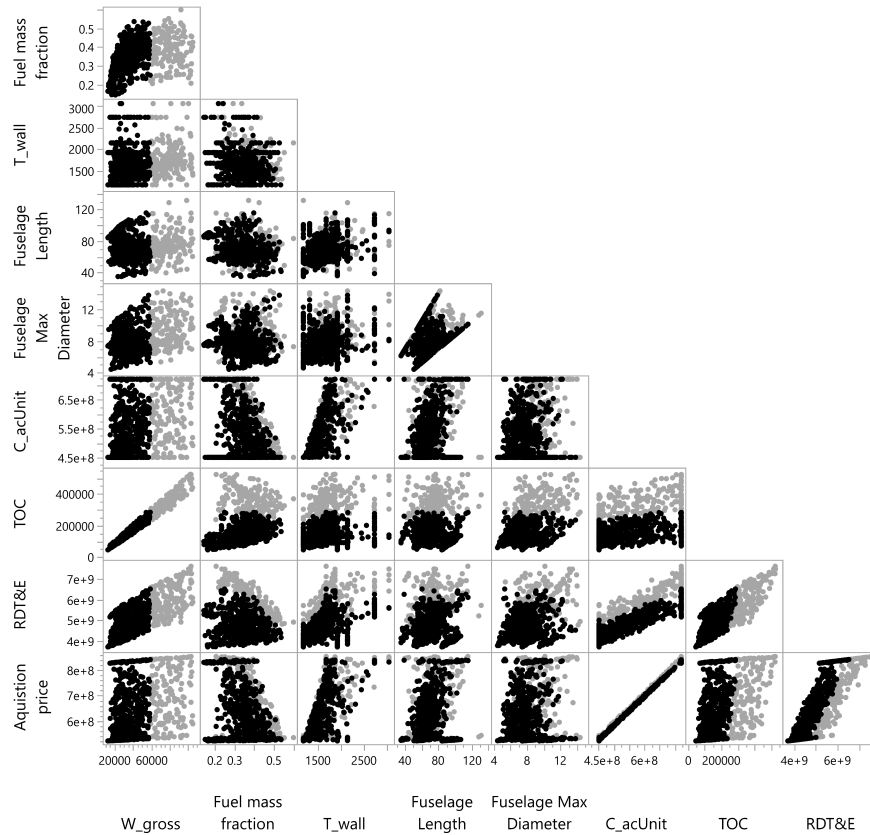


**Fig. 26 Overall scatter plot matrix: vehicles under 50,000lb**

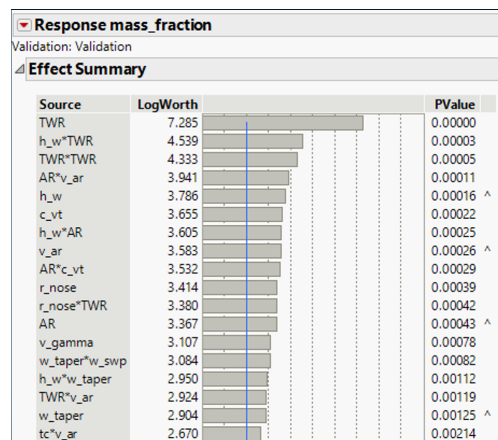


**Fig. 27 Variable importance**

- Model Fit Error (MFE)
- Actual/Residual by Predicted

These metrics provide many ways to assess the fit and predictability of the surrogate models. A visual representation of the model fits can be shown in Figure 28.



Assessing the sensitivities, there are some key relationships, one of is the Mach number. Looking at this sensitivity, almost every output increases in value with increasing Mach number. This observation makes sense as increasing speeds result in higher temperatures, cost, and complexity. After the key parameters are identified and the sensitivities are set to the desired traits of the vehicle, the next step is to down select a configuration.

## VII. Vehicle Selection

### A. Overall Design

A set of desirability functions (*e.g.*, minimization or maximization preferences) are imposed on each output parameter, allowing to find the combination of design parameters that produces an aircraft with the optimum performance relative to the mission requirements. Ideally, for our design, minimizing all of the output parameters relates to the best performing aircraft. However, there is a competing effect between the outputs for some design variables (*i.e.*, increasing the wing aspect ratio decreases the takeoff gross weight required but increases the total operating mission cost) that needs to be taken into consideration. Therefore, the combination of design parameters that maximizes the desirability functions for the all the output parameters is selected. Finally, the results from this process that correspond to the best selected vehicle are presented in Table 6.

**Table 6 Selected vehicle parameters**

Design parameters	Optimum value
Fuselage height-to-width ratio	1.03
Fineness	9.98
Nose radius (m)	0.38
Wing aspect ratio	0.98
Thickness-to-chord ratio	0.02
Wing loading	110
Wing taper ratio	0.04
Wing sweep angle	53.08
Wing dihedral (deg)	-2.35
Tail volume coefficient	0.05
Tail aspect ratio	1.37
Tail taper ratio	0.07
Tail sweep angle (deg)	63.18

Most of the existing concepts for hypersonic vehicles are streamlined bodies. This choice becomes evident when considering that an infinitely thin flat plate produces the least amount of drag per unit area (perpendicular to the flow) and therefore, these concepts aim for designs that perform substantially well at high speeds but realistically underperform when climbing through the subsonic and supersonic regimes using self-powered airbreathing engines. Figure 30 shows the final design of the UPRISE vehicle which follows a similar pattern as the existing concepts. However, when

designing UPRISE, optimization on the subsonic and supersonic phases was taken into consideration, therefore resulting in a vehicle that is more robust than a singular high speed design.

**UPRISE Configuration**

**Note:** All dimensions in feet

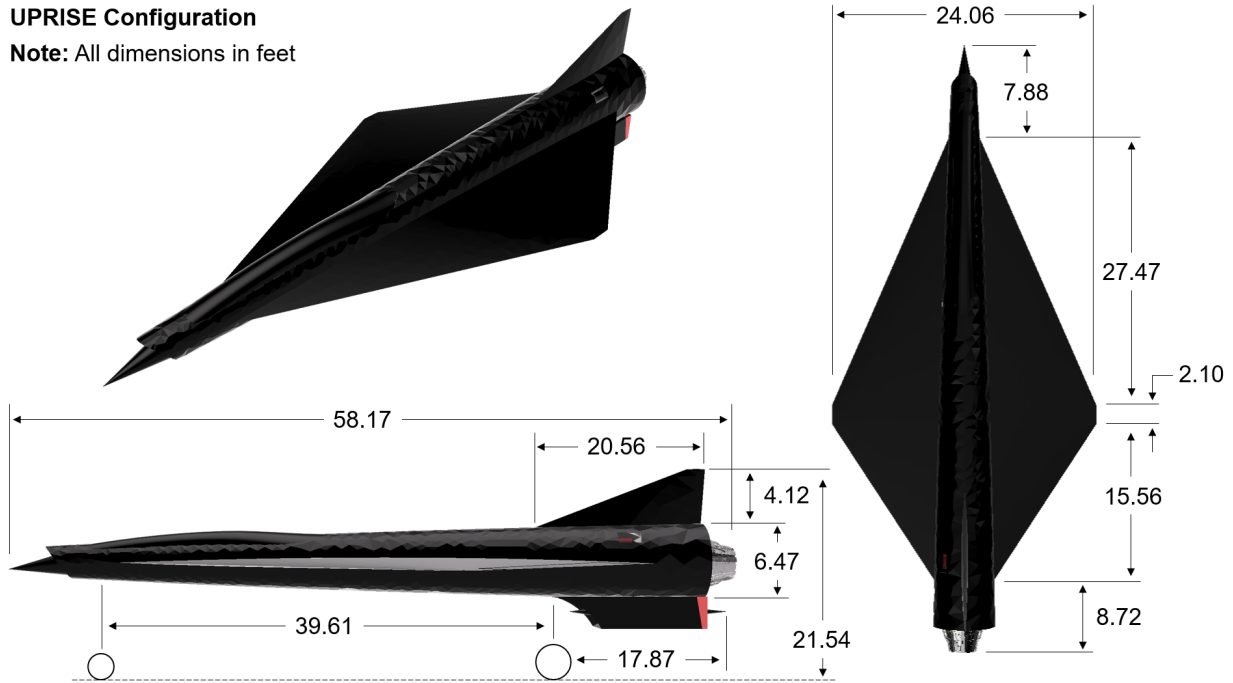


**Fig. 30 Optimal UPRISE configuration**

Other considerations are the constraints imposed on takeoff from and landing on a runway measuring 8000 ft. This requires to have a wing big enough to fly at the required approach speed in order to land in the runway. Notice that the optimum vehicle corresponds to an UPRISE 1 configuration type, thus suggesting that a dart-like design provides a better overall performance than the classic (UPRISE 2) design for the required mission profile. Table 7 shows the output parameters for the selected configuration for both the objective and threshold mission requirements, as well as an intermediate requirement to show the sensitivity of the design. Note, that the final configuration is consistent with the design that fulfills the objective mission.

A key challenge for selecting the optimal UPRISE configuration, is considering the space allocation within the fuselage. This not only involves placing components into a practical layout, but also involves ensuring that the dimensions are correct, optimal, and compatible with the vehicle requirements. One of the most important considerations is placing components in such a way that the vehicle maintains static stability at high Mach numbers during cruise. The calculations required for stability considerations for the final UPRISE vehicle can be found in VII.F

Another consideration is allocating space for a rectangular payload inside the round fuselage. To do this, the additional area is calculated by considering the difference between width of the payload box and the equivalent half-diameter of the fuselage. This calculation also includes space for the 2000 W battery needed to power the ISR

**Table 7 Selected vehicle parameters**

Output parameters	Mission requirements		
	M = 5 $h = 80000$ ft $r = 2500$ nmi	M = 6.5 $h = 90000$ ft $r = 2750$ nmi	M = 8 $h = 100000$ ft $r = 3000$ nmi
$W_{gto}$	53339 lb	67002 lb	76173 lb
Fuel mass fraction	0.43	0.36	0.31
$S_{ref}$	557 ft <sup>2</sup>	778 ft <sup>2</sup>	855 ft <sup>2</sup>
Maximum temperature of the wall	1359 K	1573 K	1754 K
Fuselage length	59.94 ft	60.1 ft	58.17 ft
Fuselage maximum diameter	6.28 ft	5.61 ft	6.13 ft
$C_{unit}$	\$ 453 M	\$ 584 M	\$ 716 M
TOC	\$ 242,154	\$ 296,241	\$ 394,743
RDT&E	\$ 4.79 B	\$ 5.71 B	\$ 6.57 B
$C_{vehicle,aq}$	\$ 547 M	\$ 713 M	\$ 858 M

payload. Therefore, the total payload weight and volume used in the computations are 1200 lb and 200 ft<sup>3</sup> respectively. This process inevitably yielded some empty space that can be considered useful for the aircraft electronics, equipment, and hydraulics components as presented in Table 8. A visual of the internal layout can be shown in Figure 31.

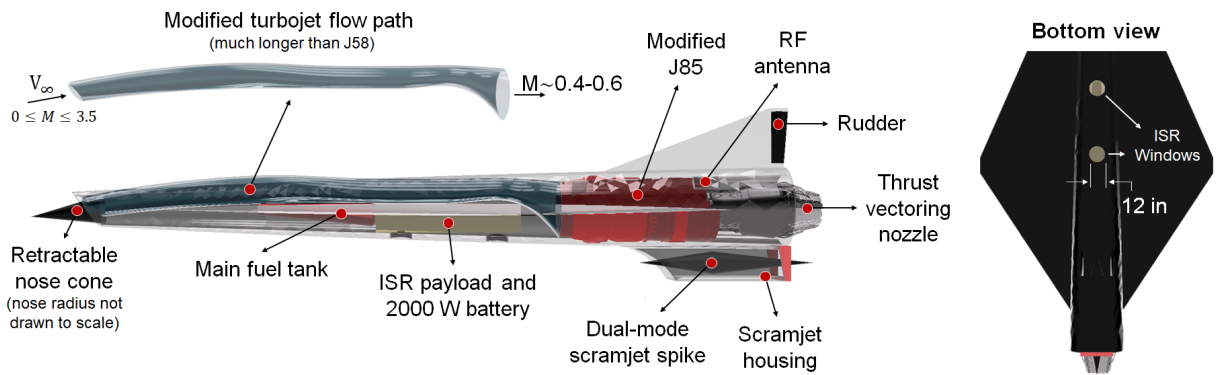


**Fig. 31 Internal layout for the UPRISE optimal configuration**

## B. Weight Breakdown

As the mission requirements become more strict (e.g., increasing Mach number, altitude and range), it is expected that the optimum takeoff gross weight, and consequently the weight of most components, increases in order to account for the more constraining conditions. This is because a higher gross weight is often associated with an increase in performance by allowing to carry more fuel and have a more robust structure. Table 8 supports this statement by showing how the weight of a vehicle changes depending on the sizing requirements for the optimum set of design parameters shown in Table 6. These results suggests that increasing the weight of the vehicle will enable the more

constraining mission phases, even if the total amount of fuel remains relatively constant. Notice that these results do not limit the ability of smaller vehicles to run the more constraining missions. However, these vehicles will most likely underperform because they will be operating outside their design conditions.

**Table 8 Vehicle weight breakdown by component and category**

<b>Component/Category</b>	<b>Threshold (lb)</b>	<b>Intermediate (lb)</b>	<b>Objective (lb)</b>
Fuselage	2712	5028	5645
Wing	2008	3303	3460
Vertical Stabilizer	266	488	585
TPS	4961	11153	17265
Landing Gear	1884	2435	2812
Thrust Structure	126	198	281
<b>Total Structural Weight</b>	<b>11957</b>	<b>22605</b>	<b>30048</b>
Turbojet	450	465	484
Scramjet	1716	3074	5202
Propellant	22936	24121	23614
Fuel Tanks	3576	3761	3682
<b>Total Propulsion Weight</b>	<b>28678</b>	<b>31421</b>	<b>32982</b>
Hydraulics	221	265	292
Electrical System	750	841	890
Equipment	10533	10670	10761
<b>Total Subsystems Weight</b>	<b>11504</b>	<b>11776</b>	<b>11943</b>
<b>Payload + Battery</b>	<b>1200</b>	<b>1200</b>	<b>1200</b>
<b>Takeoff Gross Weight</b>	<b>53339</b>	<b>67002</b>	<b>76173</b>

### C. Propulsion

As discussed in section V.C, the UPRISE concept uses two engines: a modified J85 turbojet and a dual-mode scramjet (*e.g.*, a scramjet designed to operate in both ramjet and scramjet modes). This propulsion system allows for the requirements (Mach, altitude, range, reusability) to be met with the least penalty due to weight, by having an engine that can produce enough thrust to overcome the effect of weight and drag at any point in the mission. The location and relative size of both engines can be seen in Figure 32.

The main objective for using a turbojet, or any other similar engine type, is to take the aircraft to a point in the mission (Mach number and altitude) where the flow conditions enable the use of the scramjet. However, since most of the mission is dedicated to the cruise phase under the scramjet power, the aircraft must carry the additional weight of the turbojet. This is the penalty associated to taking off from the ground using a self-powered airbreathing propulsion system. As the aircraft weight and size increases, so does the thrust required to be produced by the engine and therefore such engine needs to be scaled in order to accommodate the new size. However, any off-the-shelf J85 engine is severely limited to Mach 3, 60000 ft by optimum design. Any speed greater than Mach 3 will yield temperatures too hot that will

**UPRISE Propulsion Systems**

**Note:** All dimensions in feet

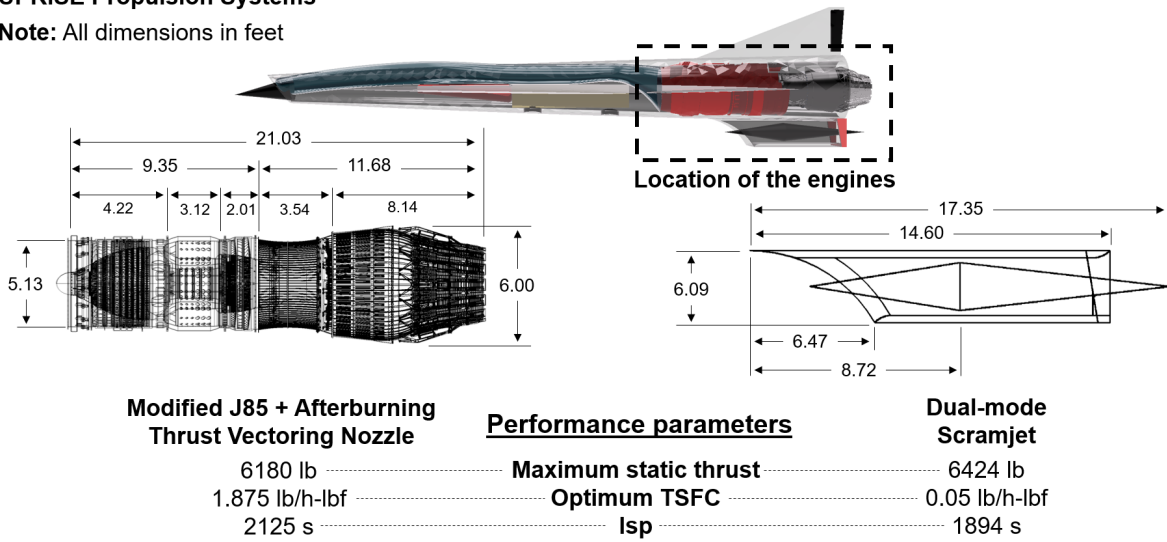


**Fig. 32 Engines location, size, and performance parameters**

melt the last stage of the compressor. Therefore, in order to accommodate for the additional increase in Mach number to reach a point where the scramjet can turn on, the cycle of the J85 is modified in a way similar to the architecture of the J58. Here, after Mach 2, air is bled from the fourth stage of the compressor (9 stages in total) directly into an afterburning chamber. This allows for cooling the flow at the last stage and obtaining the thrust required without melting the engine. For this process, an adiabatic component is assumed on the transition from compressor to afterburner. The result of this process is an engine that behaves very similar to the J58 but with the efficiency of the J85. Additionally, this engine is much lighter in weight (~5500 lb less). Figure 33 shows the performance of the modified engine for different flight conditions.

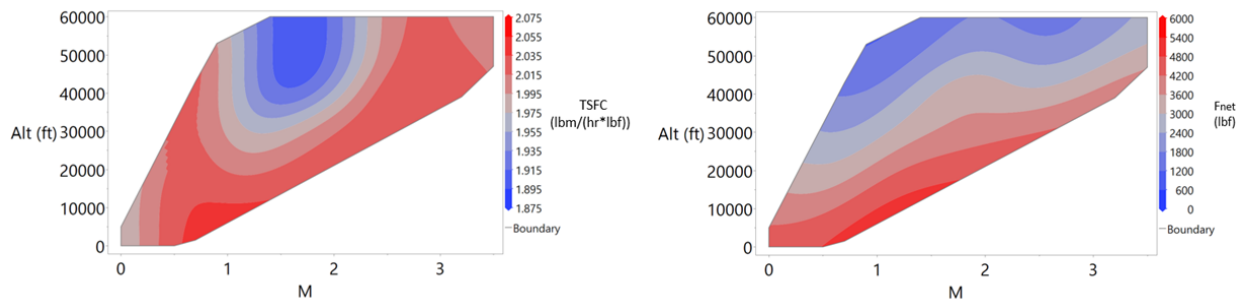


**Fig. 33 Performance parameters of the modified J85 turbojet at different flight conditions**

## D. Aerodynamics

The aerodynamic performance of the aircraft substantially changes as a function of the Mach number and altitude. Figure 34 shows the variation on the drag polar for the final design at different mission phases. At takeoff at sea level, the amount of lift generated by the wing compared to the amount of drag produced is substantially low. This is because the aircraft is designed for high speed and altitude flight, hence, a loss of performance in the other aspects is expected. At Mach 3.5 at an altitude of 60,000 ft (at the transition from turbojet to (sc)ramjet operation) during the supersonic flight regime, substantial improvements in performance can be observed with lift-to-drag ratios greater than three times the takeoff subsonic flight conditions. Certainly, the best performance of the aircraft is obtained when flying at hypersonic speeds, especially at around Mach 6 at 90000 ft. Through exploring the drag polars, this condition yields the best aerodynamic propulsion. This should not be a surprise since the aircraft is designed for hypersonic flight. Interestingly, looking at the most constraining design condition (*e.g.*, Mach 8 at 100000 ft), the aircraft aerodynamic performance is reduced compared to the performance at the slightly lower Mach number. This might be due to the effect of higher speed flow impinging on the equivalent surface generating higher overall pressure forces on the aircraft which increase the drag. Alternatively this observation could be due to the effect of unstable pressure waves on the lifting surfaces, however this phenomenon is not considered in this design. This shows that while the aircraft can operate at these high speeds, it is most efficient at a specific set of flight conditions.

Besides the drag polars, there are additional metrics to assess the aerodynamics performance of the vehicle, particularly at cruise. One of such metrics is the lift to drag ratio at varying angles of attack. Looking at cruise in particular, Figure 35 can be generated.

The L/D vs. Alpha plot is significant for many reasons. First, it shows the expected cruise performance of the vehicle. A L/D ratio around 5 is higher than anticipated for this vehicle but certainly not unheard of. As can be shown, all the conditions have very similar performance with the peak lift to drag ratio occurring at approximately 5 degrees angle of attack. Given this information, the vehicle cruise conditions can be set to achieve optimal efficiency. Looking closer at the plot, the specific flight conditions need to be found for cruise. Zooming in to Figure 35, Figure 36 can be generated.

As shown in Figure 36, it can be shown the aerodynamic performance decreases with increasing speed and altitude. This assessment is consistent with that of the drag polar analysis.

Along with the drag polars and lift to drag analysis, the pressure and local heating contours can be assessed as well. Analyzing the contours provides a quick check to the feasibility of the design in regards to pressure and local heating. Shown in Figure 37 are the pressure contours at 10 degrees angle of attack.

As shown in the figures, the pressure trends are correct. At positive angles of attack, the final vehicle proves to have low pressure on the upper surface and high pressure on the lower surface, as expected. Seeing that pressure is correct, local heating can be accessed.

As shown in the contour, the leading edges of the final vehicle experience excessive heating, as predicted. Using this



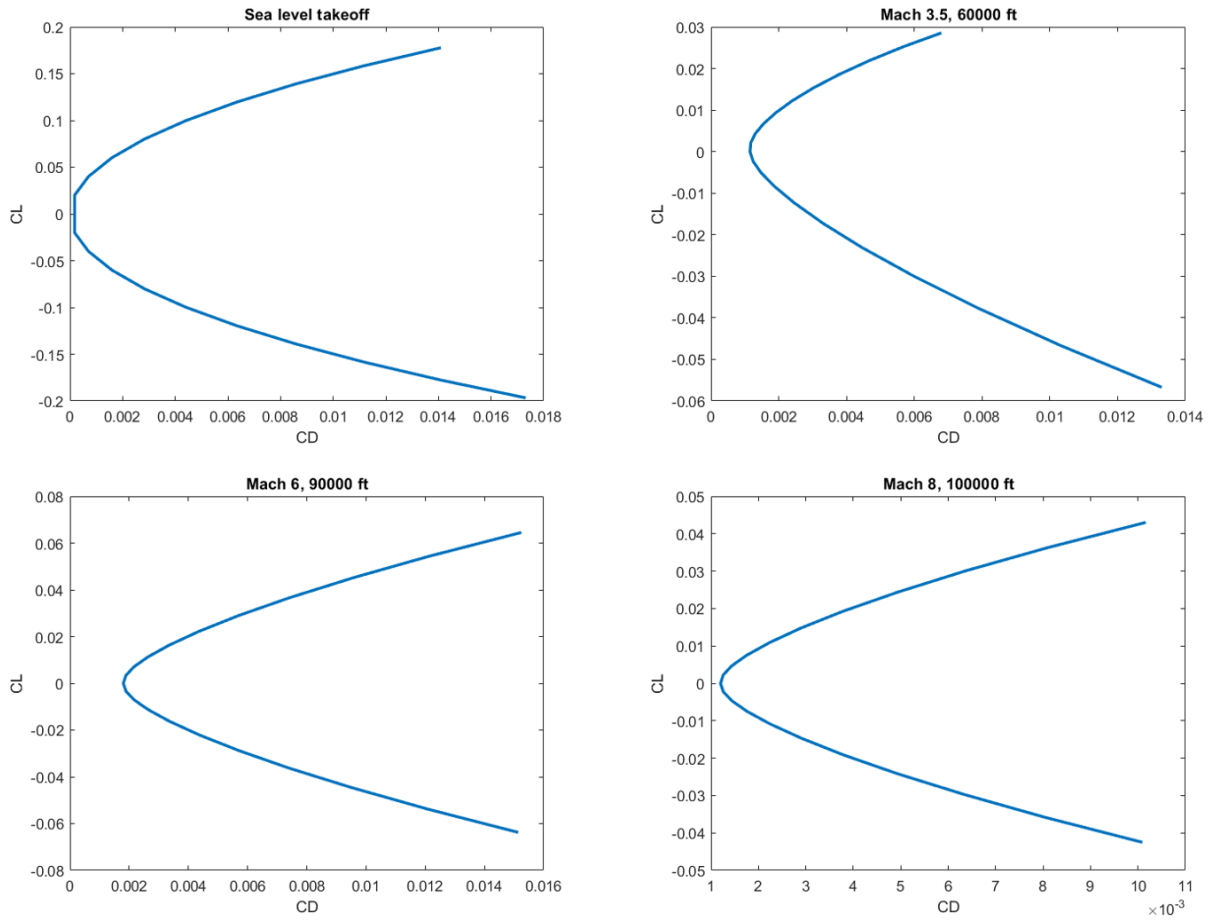


**Fig. 34 Aircraft aerodynamic performance for different flight conditions**

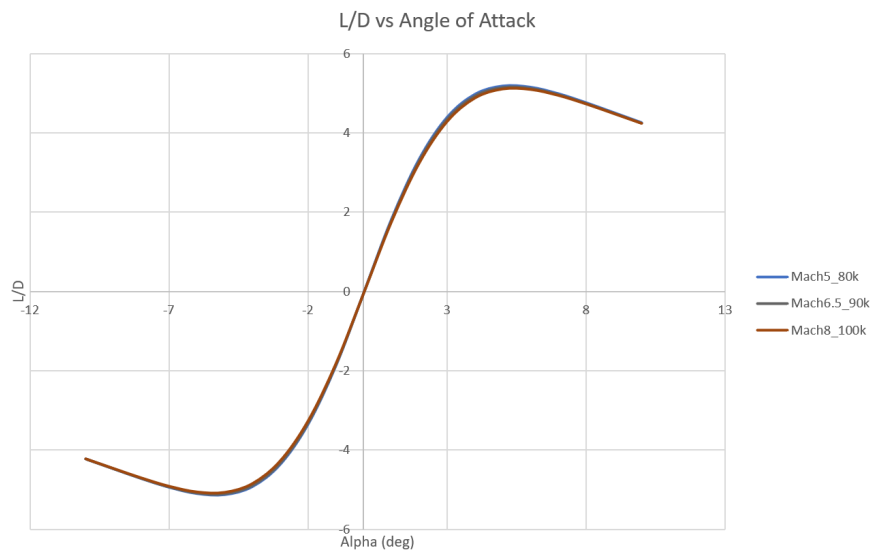


**Fig. 35 Aircraft aerodynamic performance at cruise**

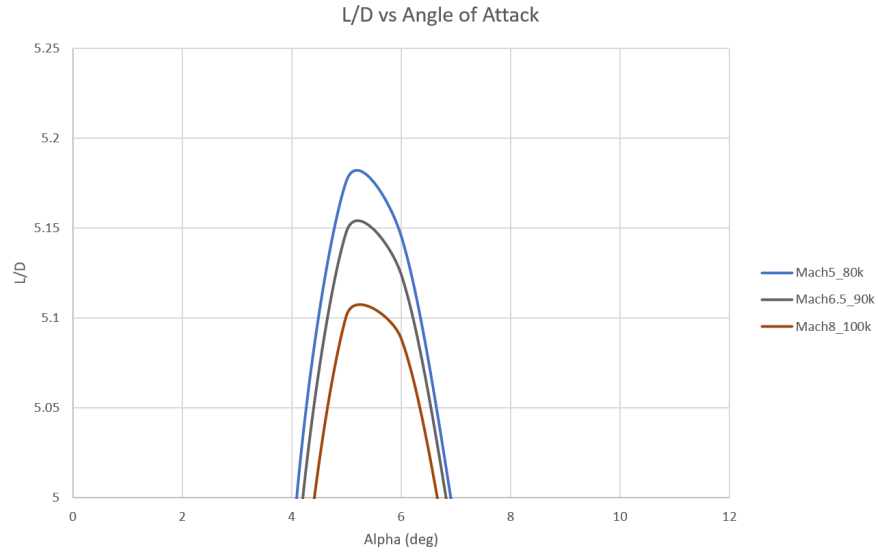


**Fig. 36 Aircraft aerodynamic performance at cruise**

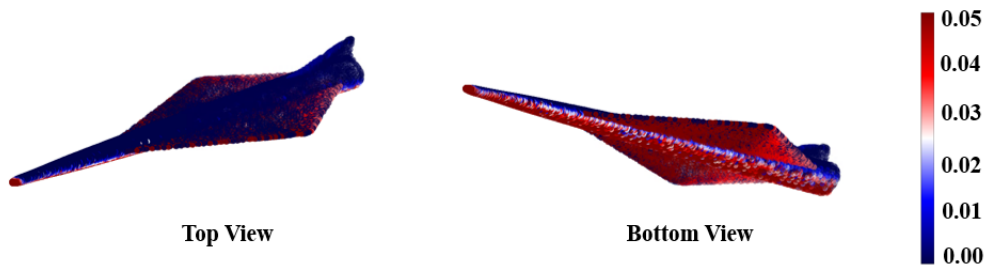


**Fig. 37 Pressure contour: 10 degrees angle of attack**

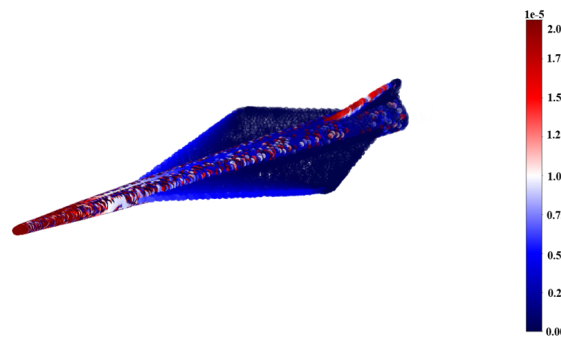


**Fig. 38 Heat transfer coefficient contour: 0 degrees angle of attack**

contour, the location of the RF antenna can be placed as shown in Figure 39.

Using the local heating contour as a guide, the RF antenna can be placed in an area of minimal heat flux, as shown to be the green region in Figure 39. At this location, the antenna is least likely to experience the extreme heating that may cause communication blackout.

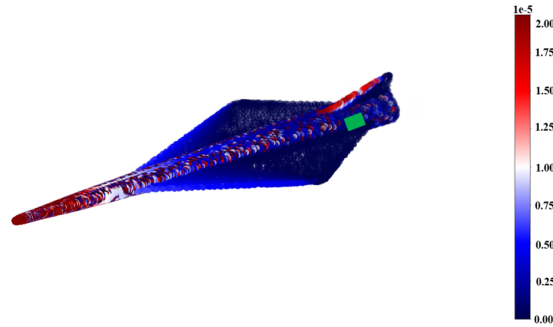


**Fig. 39 Heat transfer coefficient contour 0 AoA: RF antenna location**

## E. Mission Analysis

Having assessed the geometry, propulsion, and aerodynamics of the vehicle, the mission analysis can be taken into consideration. The mission profile subsequently considers the takeoff, climb, cruise, and landing segments, each with different characteristics and requirements.

### 1. Takeoff

In order for the UPRISE aircraft to perform its mission, it first needs to be able to takeoff. The aircraft is designed to takeoff from an 8000 ft runway, modeled by constraining the flight path angle to be zero as the aircraft accelerates until enough lift produced by the wing to balance the weight. This must happen within 8000 ft for the aircraft to be a feasible consideration. An important consideration is avoiding tail strike as the aircraft rolls in order to climb. Shown in Figure 40 is a visual of the detailed analysis the mission analysis module performs to avoid tail strike.

### 2. Climb

As described in section VII.E, the climb phase is modeled as a constraint optimization problem to minimize the time it takes to climb. The resulting process is illustrated in Figure 41.

As time progresses in the climb segment of the mission, the ideal speed and altitude behaviors are found to be linear. Looking at the mass variable, it is shown that as the climb progresses, the mass of the aircraft decreases at a nearly linear rate. These observations tracks well with reality in comparison to other high-speed airbreathing vehicles. From the results, it can be observed that the minimum time to climb in this case, 986 s, is not obtained by climbing at a constant speed and flight path angle. Instead, the aircraft first accelerates while maintaining a constant altitude at level flight until it reaches approximately Mach 0.85 where the drag force starts increasing (the aircraft is getting closer to the transonic regime and the critical Mach number). At this point, the aircraft climbs at a constant speed until it reaches an altitude of about 30000 ft and then performs a small dive until it reaches about 25000 ft, which it does in order to gain speed and pass through the transonic regime easier. Then, it slowly starts climbing back to about 9000 m while increasing its speed, with the objective of increasing the energy (at this point, the energy overall, that is kinetic plus potential will be

**UPRISE Takeoff and Tail Strike Avoidance**

**Note:** All dimensions in feet

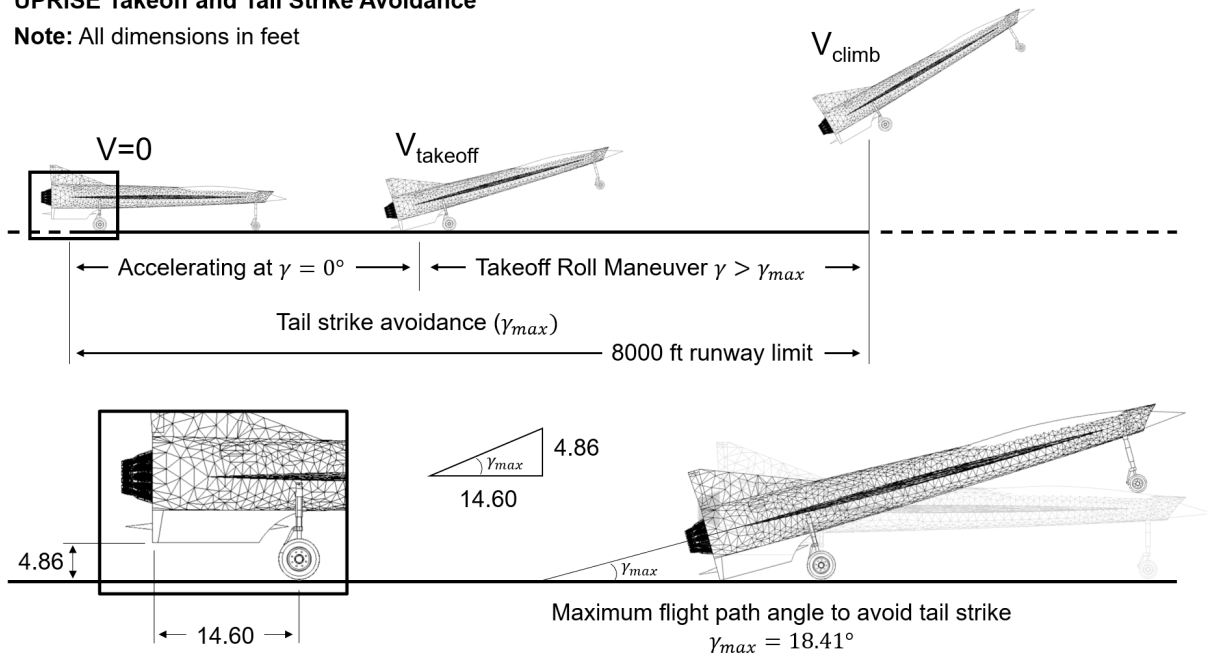


**Fig. 40 Takeoff and tail strike avoidance**

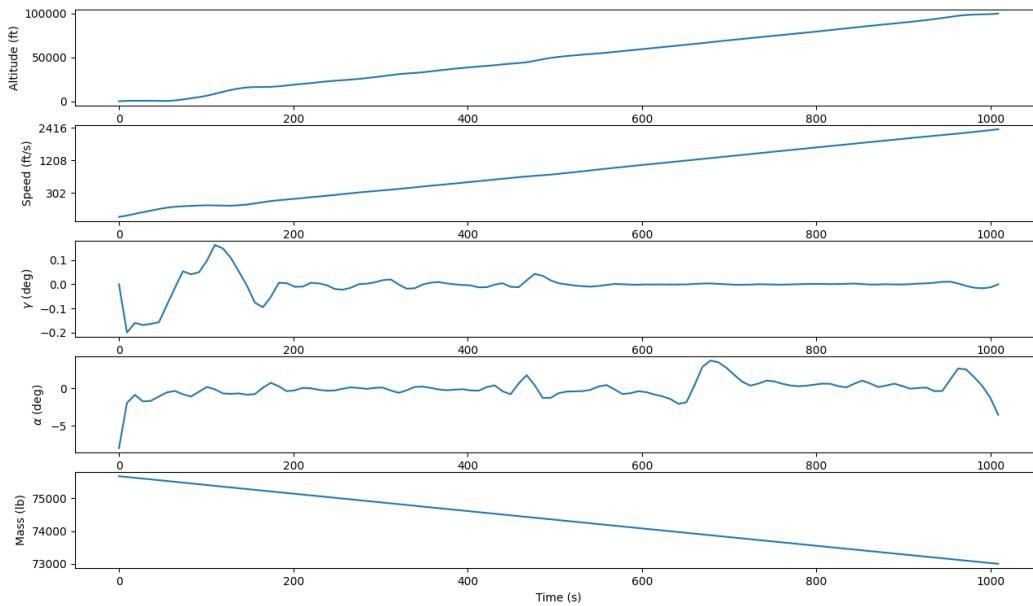


**Fig. 41 Climb trajectory of the aircraft**

equal to the final energy of the objective). Finally, the aircraft climbs while accelerating until it reaches the objective conditions (i.e., Mach 5+ and 80000+ ft at level flight). An interesting analysis can be performed by looking at the change of velocity with altitude, which supports the previous statements and is shown in Figure 42.

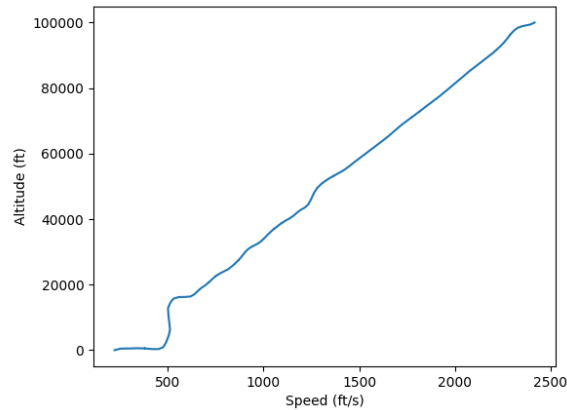


**Fig. 42 Altitude with respect to velocity during climb segment**

### 3. Landing Performance

A critical performance criteria for designing the UPRISE aircraft is its ability to fly at low speeds in order to land successfully in less than 8,000 ft on a conventional paved runway. Requirements in mind, the UPRISE landing gear is modeled as a derivative concept of the SR-71 landing gear. The SR-71 landing gear allowed the aircraft to land in approximately 3609 ft while aiding the stopping with a parachute deployed right after touchdown. However, considering that even including the parachute, this tested landing distance only represents 55% of the required runway length. Thus, it is reasonable to design the UPRISE landing gear configuration without a parachute but still make considerations for the differences in weight and wing loading with respect to the SR-71. Figure 43 shows the dimensions and location of the landing gear for the UPRISE configuration.

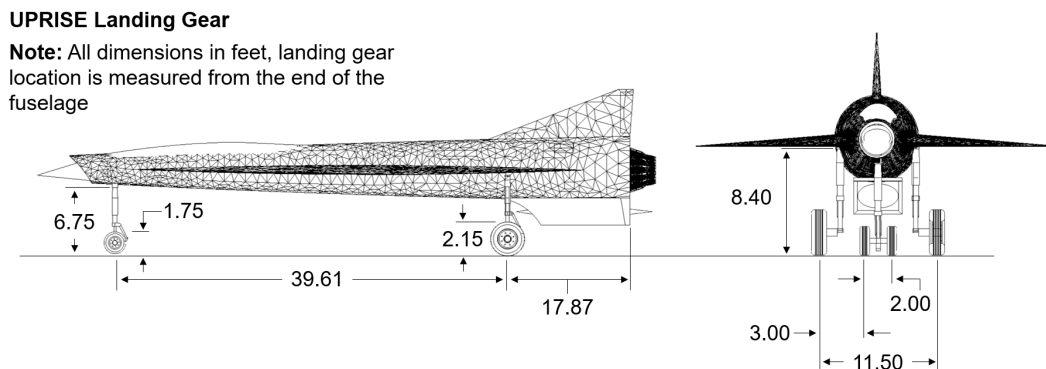


**Fig. 43 Landing gear location and dimensions**

While certain considerations are baked-in to the analysis for the landing requirement, it is still important to calculate the expected performance. To perform this analysis, Mattingly's Master Equation can be derived to create an expression for the landing ground roll distance [22]. Before diving into the mathematics, it is important to understand what a

landing profile looks like, as shown in Figure 44.

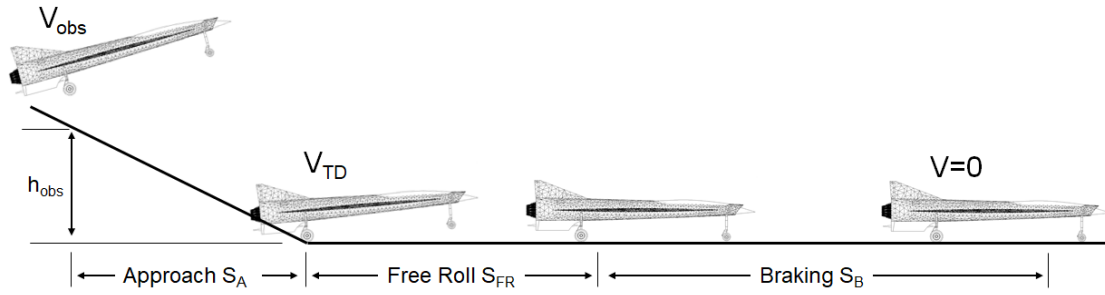


**Fig. 44 Generic landing profile**

Given that landing in the space allotted is difficult as is, the assumption is made that there is no obstacle for the aircraft to clear at landing. Thus, the only landing considerations are the free roll distance, braking distance, and total ground roll distance. Looking first at the free roll distance, this segment is typically dedicated to the aircraft "aerobraking" before engaging the brakes. The purpose of the free roll is to bleed energy away from the brakes so there is a lower likelihood of failures, fires, etc. due to overloading the brakes. The expression for free roll distance is shown below.

$$S_{FR} = t_{FR} \times V_{TD} \quad (33)$$

As Equation 33 shows, the free roll distance is simply the time of the free roll multiplied by the touchdown velocity, which in our case was found to be 443 ft/s from the mission analysis. Typically, the aircraft free rolls for around 3 seconds before the brake is engaged. Having the free roll accounted for, the braking distance can be calculated. The expression for the braking distance can be shown below.

$$S_B = \frac{1}{2B} \ln \frac{A - BV^2}{A} \quad (34)$$

where

$$A = g \left( \frac{T}{W} - \mu \right) \quad (35)$$

and

$$B = \frac{g}{W} \left[ \frac{1}{2} \rho S (C_D - \mu C_L) \right] \quad (36)$$

In Equation 34,  $V$  represents the speed at braking which is normally 80% of the touchdown speed. This speed reduced accounts for energy loss due to aerobraking and ground friction. In Equation 35,  $g$  represents gravity,  $T$  represents the static thrust at the time of braking,  $W$  represents the weight of the aircraft, and  $\mu$  represents the braking

friction coefficient. In this particular case, it is assumed that no thrust is applied at the time of braking thus making that term zero. Additionally, the braking coefficient is assumed to be 0.4 which is very typically for an aircraft of this category and class. Moving on to Equation 36,  $\rho$  represents sea level density and  $S$  is the wing area of the vehicle. Having all assumptions and variables accounted for the total ground roll length is 7,432 ft thus meeting the 8,000 ft requirement.

While the ground roll distance can meet requirements on a dry, fair weather, day, it is important from an operations standpoint to know if the vehicle is operable in wet runway conditions. To perform this analysis, the same procedure is followed as before but assumptions change. Using models from the FAA [23], the braking friction coefficient can be expressed below. Note this expression is for a tire of 300 psi which is standard for vehicles of this size.

$$\mu = -0.0401\left(\frac{V}{100}\right)^3 + 0.263\left(\frac{V}{100}\right)^2 - 0.611\left(\frac{V}{100}\right) + 0.614 \quad (37)$$

Using Equation 37 for a 300 psi tire, the braking friction coefficient comes out to approximately 0.1 as opposed to the dry conditions at 0.4. Substituting the new value, the total ground roll distance on a wet runway is calculated to be 16,500 ft which shows that this design is only operable in dry, fair weather, conditions.

## F. Stability and Control

One important consideration to complete the analysis of the UPRISE configuration is to determine the overall stability of the aircraft, especially at the cruise conditions where trimmed flight is often desired. Based on the weight of the individual components and the distance from the nose in the direction of the fuselage length, the center of gravity can be calculated using the expression below for each component in Table 8.

$$c.g. = \frac{\sum_{i=1}^n m_i x_i}{W_{gto}} \quad (38)$$

This point is a geometrical/structural property of the aircraft and changes by 1) burning fuel throughout the mission and 2) changing the internal layout. Essentially, the center of gravity is the average location of the weight of an object. The second part involves calculating the aerodynamic center at the hypersonic cruise conditions using the aerodynamics concepts. This point denotes the location at which the moments applied to the aircraft are zero and it does not change with angle of attack. Ideally, one of the stability considerations is that the center of gravity must be in front of the aerodynamic center in order for the aircraft to be statically stable. This means that once a disturbance occurs in level flight, a statically stable aircraft will counteract with a moment in the opposite direction to the disturbance in order to return to the equilibrium position. Table 9 presents the results for the static stability analysis for the UPRISE configuration.

The second consideration are the sizes of the control surfaces needed to maneuver the aircraft at any point in the

**Table 9 Static stability analysis**

	<b>Aerodynamic Center (ft)</b>	<b>Center of Gravity (ft)</b>	<b>Margin (%)</b>
Fully loaded vehicle	34.32	31.51	8.19
Vehicle + Reserve Fuel	34.32	33.85	1.37
Empty Vehicle	34.32	34.28	0.11

mission. The UPRISE configuration contains two types of control surfaces: elevons and rudder. The elevons are located at the trailing edge of the wing, and allow to change the pitch of the aircraft as well as performing roll maneuvers. Elevons are essentially a combination between elevators that control the lateral movement of the aircraft and ailerons that control the rolling motion, hence their name. The size of the elevons are determined by the maneuverability of the aircraft, meaning that aircraft that require large maneuvers also require larger elevons. Since the UPRISE configuration does not require neither quick nor constant changes in maneuvers, the size of the elevons are quite small. In fact, most of the consideration behind their size is determined by the climb phase in order to account for the changes in angle of attack required to climb to the cruise conditions. The second type of control surface, the rudder, is used to provide lateral yaw control of the aircraft. This part presents a crucial role in the cruise phase by ensuring that the aircraft can travel in a rectilinear trajectory with minor disturbances. Considering that the UPRISE configuration does not require many maneuvers (aircraft trim is calculated during the cruise condition and the control surfaces are set to a given position that is not considered dynamically) and assuming that there are no external disturbances, a large rudder is not crucial to maintain control. Figure 45 shows the location of these control surfaces and details about their size.

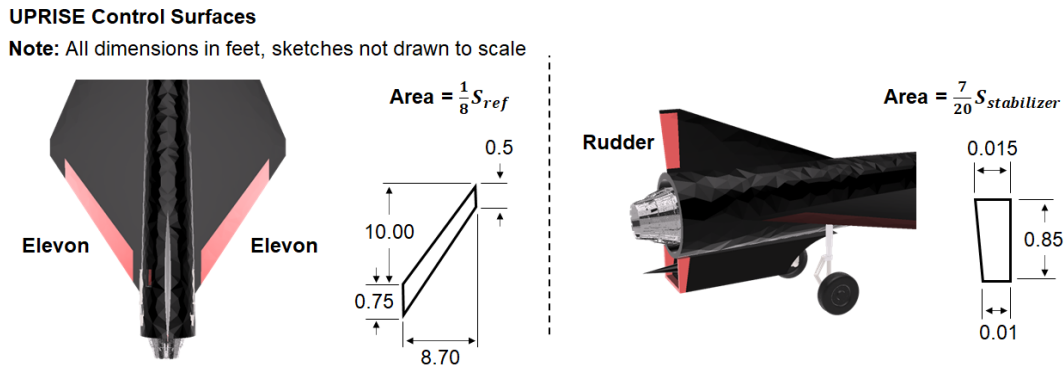


**Fig. 45 Control surfaces size and location**



## VIII. Conclusion

The UPRISE vehicle is an ISR vehicle designed to be operable from subsonic to hypersonic speeds with airbreathing propulsion. It has a range of 3000 nautical miles with a cruise speed of Mach 8 and cruise altitude of 100,000 ft, thus meeting the objective requirements in the RFP. The total cost per vehicle in 2022 dollars is approximately \$716 million with total operating costs per sortie at around \$395,000. Comparing to previous programs, the cost of a single SR-71 is approximately \$330 million when converted to 2022 dollars. While the UPRISE vehicle cost is over double that of the SR-71, the UPRISE vehicle is much more complex due to its hypersonic capabilities and stringent reusability requirements.

The report shows the highly complex and coupled nature of hypersonic vehicle design as well as a robust approach to meet requirements. Future work on the UPRISE vehicle will involve deeper trade studies, increasing MDA efficiency, and more elaborate validation with high-fidelity tools.

**Table 10 UPRISE compliance to RFP requirements**

	<b>Requirements</b>	<b>UPRISE Performance</b>	<b>Requirement Met</b>
<b>Cruise Speed</b>	Threshold: Mach 5 Objective: Mach 8	Mach 8	Yes
<b>Range</b>	Threshold: 2,500 nmi Objective: 3,000 nmi	3,000 nmi	Yes
<b>Cruise Altitude</b>	Threshold: 80,000 ft Objective: 100,000 ft	100,000 ft	Yes
<b>Runway Field Length</b>	Max Length = 8,000 ft Conventional Paved Runway	7,432 ft	Yes
<b>Reusable</b>	Turn around time between sorties < 24 hrs	Airbreathing Propulsion Non-ablative TPS	Yes
<b>Mission Profile</b>	Capable of one way and round trip	Round-trip: 2g turn One-Way: Range Met	Yes
<b>ISR Payload</b>	Dimensions: 3' x 3' x 12' Weight: 1000 lb 2 Downward facing windows: 12" diameter Windows: EO/IR transparent and contiguous to payload space Power Required: 2000 Watts	Accounts for: Payload Weight Payload Volume Local Heating Battery Required	Yes
<b>RF Antenna</b>	Window size: 1' x 2' Location: Either side of fuselage	Placed at rear of fuselage	Yes
<b>Production Run</b>	RDTE: 5 aircraft and 2 ground stations 10 year production run 10 aircraft/year and 2 ground station/year IOC no later than 12/2030	Accounts for: RDTE Costs Acquisition Costs Misc. Program Costs	Yes

## References

- [1] AIAA, "2021-2022 Graduate Team Missile Systems Design Competition - Reusable Penetrating Hypersonic ISR," *AIAA* [https://www.aiaa.org/docs/default-source/uploadedfiles/education-and-careers/university-students/design-competitions/graduate-team-missile-systems-graduate\\_design\\_competition\\_2021---2022.pdf?sfvrsn=2c9c3ba5\\_0](https://www.aiaa.org/docs/default-source/uploadedfiles/education-and-careers/university-students/design-competitions/graduate-team-missile-systems-graduate_design_competition_2021---2022.pdf?sfvrsn=2c9c3ba5_0), August 2021.
- [2] Childress-Thompson, Rhonda, Dale Thomas, and Philip Farrington, "A Framework for Assessing The Reusability of Hardware (Reusable Rocket Engines)," *NASA*, <https://ntrs.nasa.gov/api/citations/20170000606/downloads/20170000606.pdf>, 2016.
- [3] Peter Merlin, "Blackbird Flight Hours," *sr-71.org*, <https://www.sr-71.org/blackbird/flighthours.php>, 2006.
- [4] Chen, D., Li, Y., Guo, J., and Li, Y., "Estimation of hypersonic vehicle weight using Physics-Informed neural network supported by knowledge based engineering," *Expert Systems with Applications*, Vol. 195, 2022, p. 116609.
- [5] Choi, Y., Yost, M. F., Lerner, E. W., and Driscoll, J. F., "Scramjet Performance Computed for a JP-7-Fueled Generic X-51 Vehicle," *Journal of Propulsion and Power*, 2022, pp. 1–11.
- [6] Kevin Bowcutt, "Physics Drivers of Hypersonic Vehicle Design," *AIAA* <https://arc.aiaa.org/doi/pdf/10.2514/6.2018-5373>, September 2018.
- [7] John David Anderson Jr., "Fundamentals of Aerodynamics," *Tata McGraw-Hill Education*, 2010.
- [8] John David Anderson Jr., "Hypersonics and High Temperature Gas Dynamics," *AIAA*, 2000.
- [9] Josue Lopez, "Aerodynamic Forces and Heat Transfer of Sphere and Sharp Cone In Hypersonic Flow," *AIAA*, May 2014.
- [10] KC Daoulas, Marcus Muller, "Single chain in mean field simulation: Quasi-instantaneous field approximation and quantitative comparison with Monte Carlo simulations," *The Journal of Chemical Physics*, 2006.
- [11] E. M. Repic, "A methodology for hypersonic transport technology planning," *Rockwell* <https://ntrs.nasa.gov/api/citations/19730023221/downloads/19730023221.pdf>, September 1973.
- [12] Forecast International, "Pratt Whitney F135 Turbofan Engine," *Powerweb* <http://fi-powerweb.com/Engine/PW-F135.html>, 2020.
- [13] Mike Snead, "Assessing the practicality of scramjet-powered, single-stage aerospaceplanes," *The Space Review* <https://thespacereview.com/article/1092/1>, March 2020.
- [14] "Jet A1 Price Today," *jet-a1-fuel* <https://jet-a1-fuel.com>, April 2022.
- [15] "Airline Operating Costs and Productivity," *ICAO* <https://www.icao.int/MID/Documents/2017/Aviation%20Data%20and%20Analysis%20Seminar/PPT3%20-%20Airlines%20operating%20costs%20and%20productivity.pdf>, February 2017.

- [16] “Independent Market Study Commercial Hypersonic Transportation,” *Bryce Tech* <https://ntrs.nasa.gov/api/citations/20210015471/downloads/SAIC%20BryceTech%20Commercial%20Hypersonics%20Transportation%2020210506.pdf>, February 2017.
- [17] Obaid Younossi, Michael Kennedy, John Graser, “Military Airframe Costs The Effects of Advanced Materials and Manufacturing Processes,” *RAND Corp.* [https://www.rand.org/pubs/monograph\\_reports/MR1370.html](https://www.rand.org/pubs/monograph_reports/MR1370.html), 2001.
- [18] Tom Benjamin, “The Real Cost of Tooling,” *MSC Direct* <https://www.mscdirect.com/betterMRO/metalworking/real-cost-tooling>, 2021.
- [19] Dan Gettinger, “Drone Spending: the MQ-9 Reaper,” *Drone Center* <https://dronecenter.bard.edu/drone-spending-the-mq-9-reaper/>, October 2015.
- [20] “Reducing the Time and Cost of Testing Engines,” *NASA* <https://ntrs.nasa.gov/api/citations/20050031186/downloads/20050031186.pdf>, January 2004.
- [21] Keith Hartley, “Estimating Military Aircraft Production Outlays: The British Experience,” *Royal Economic Society* <https://www.jstor.org/stable/2229796?seq=1>, December 1969.
- [22] Jack Mattingly, “Aircraft Engine Design,” *AIAA*, 2002.
- [23] Somil Shah, “Aircraft Braking and Runway Friction Research,” *FAA* [https://www.faa.gov/about/office\\_org/headquarters\\_offices/ang/redac/media/airports/2021/march/airports-mar2021-AircraftBrakingandRunwayFrictionResearch.pdf](https://www.faa.gov/about/office_org/headquarters_offices/ang/redac/media/airports/2021/march/airports-mar2021-AircraftBrakingandRunwayFrictionResearch.pdf), March 2021.